# Chlorine isotope data of chlorides challenge the pore fluid paradigm

Pierre Agrinier, Magali Bonifacie, Gérard Bardoux, Francis Lucazeau, Thomas Giunta, Magali Ader

# CHLORINE ISOTOPE DATA OF CHLORIDES CHALLENGE THE PORE FLUID PARADIGM

Pierre Agriner[1], Magali Bonifacie[1], Gerard Bardoux[1], Francis Lucazeau[1], Thomas Giunta[2], Magali Ader[1]

[1] Université de Paris, Institut de physique du globe de Paris, CNRS, F-75005Paris, France.

[2] IFREMER, Unité des Géosciences Marines, 29280 Plouzané, France

## Abstract

In order to examine the seawater-seafloor sediment interactions that influence the chemical composition of seawater through time, we examined hundreds of pore fluid geochemical analyses from 13 clay-rich sedimentary successions drilled by the ODP-IODP. Chemical trends such as monotonous increases in $Ca^{2+}$, and decreases in $Mg^{2+}$ and $\delta^{18}O$ with depth are traditionally interpreted to result from water-rock interaction. In this view, the release of $Ca^{2+}$ into fluids and the uptake of $Mg^{2+}$ and $^{18}O$ mainly results from the formation of low-temperature clays in the sediment and within underlying basalts. Chloride concentration profiles and isotopic compositions, however, suggest that different processes may influence pore water geochemistry. The data examined here show relatively constant chloride contents but with a systematic decrease in $\delta^{37}Cl$ of chlorides with depth from 0 permil (the seawater value) down to -8.5 permil. The $\delta^{37}Cl$ data are highly correlated with $\delta^{18}O$ (with $\delta^{18}O$ down to -5.7 permil).

The $^{37}Cl$-depletions of pore fluid chlorides are found in all studied sedimentary piles regardless of tectonic or sedimentary history. These trends cannot be explained by water-rock exchange reactions because minerals formed at low temperature have Cl contents that are too low to compensate for $^{37}Cl$ depletions observed in pore fluids. Accordingly, we hypothesize that fluid-specific processes are responsible for the $^{37}Cl$-depletions of the fluids and that $^{37}Cl$-enriched chlorides were expelled out of the sediments into the ocean. After reviewing the fluid-specific processes that are known to change the chlorine isotope ratios in chlorides, we rule out diffusion and gravitational isotope fractionations of chlorides could generate this isotope pattern. The flow of a $^{37}Cl$ -depleted fluid from the underlying basaltic basement into the sediments could explain the $\delta^{37}Cl$ data. But the mechanism that produces depletion in $^{37}Cl$ of the fluid remains unknown. It cannot be chloride exchanges between fluids and rocks.

Here we show that compaction-induced ion filtration of chlorides through clay-rich membranes can produce the observed pore fluid $^{37}Cl$-depletions, with isotope fractionation factors ranging from 1.000 to 1.008 between the chlorides of the expelled fluid (the permeate) and those of the residual fluid (the retentate). We find that smectite-rich sediments are associated with higher isotopic fractionation factors, while illite/chlorite-rich sediments are associated with intermediate values and with clay-poor sediments associated with lower values. This suggests that chlorine isotope fractionation might be controlled by surface charge associated with specific clay minerals. Our calculations show that compaction-induced filtration has the capacity to produce $^{18}O$-depletion for oxygen isotope fractionation factors between the expelled fluid and the retentate ranging from 1.000 to 1.005. $^{18}O$-enrichment in the expelled fluid is in agreement with the experimental data of Haydon and Graf (1986). Overall, although

further experimental work on both chlorine and oxygen isotopes is certainly needed, the results of this study indicate that ion-filtration should be considered as a potential mechanism for fractionating isotopic species in sediment pore waters, particularly for oxygen isotope ratios whose variations are often commonly attributed to water-rock exchange.

## I) Introduction

Water-rock interactions and transport of solutes by water are means by which chemical elements are redistributed at the surface of the Earth. Through these processes, the Earth's surface and subsurface reservoirs, such as seawater, continental crust, sediments, altered oceanic crust, were created, maintained and modified all along the Earth's history. To decipher this history, geochemical tools were developed. They include stable isotope geochemistry of traditional elements (O, H, C, N, S) and non-traditional elements (e.g., Cl, Li, B, Cu, U, Zn, Se). Although chlorine stable isotope geochemistry started in the early times of the stable isotope geochemistry, it remains an under-utilized tool. Yet, chlorine stable isotopes ($^{37}Cl$ & $^{35}Cl$) of dissolved chlorides are proved to be powerful tools to describe transport mechanism of fluids. Physical processes mainly fractionate them during fluid transports in geological media: diffusion (Eggenkamp et al., 1994; Hendry et al., 2000; Eastoe et al., 2001; Lavastre et al., 2005; Eggenkamp and Coleman, 2009; Giunta, 2015; Bernachot et al., 2017), ion filtration by fluid advection through clays (Agrinier et al., 2019), gravitational sorting (Giunta et al., 2017a), absorption (Musashi et al., 2007). They are weakly fractionated by the formation of minerals because Cl does not enter much in low-temperature alteration minerals but in evaporite salts (Eggenkamp et al., 2016; 2019) and rarely involved in redox reactions (Ziegler et al., 2001; Bonifacie 2005, Barnes and Cisneros 2012, Selverstone and Sharp 2015; Bonifacie, 2017, Giunta et al., 2017b, Gue et al., 2018). In this light, chlorine stable isotopes are an ideal geochemical tool for describing the physical history of fluids.

That way the chlorine stable isotope compositions are used to examine chlorides of low temperature pore fluids in oceanic sediments. Depletions in $^{37}Cl$ have been systematically reported in sediments of accretionary prisms of subduction zones ($\delta^{37}Cl$ ranging from -8.5 to 0 ‰ in comparison to seawater, $\delta^{37}Cl$ = 0‰; Ransom et al., 1998; Spivack et al., 2003; Deyhle et al., 2003; Godon et al., 2004a; Wei et al., 2008; Agrinier et al., 2019) and in other oceanic contexts ($\delta^{37}Cl$ down to -3.5 ‰ Hesse et al., 2000; Bonifacie et al., 2007). In the sediments of subduction zones, Wei et al. (2008) suggested the advection of exogenous $^{37}Cl$-depleted rising fluids produced at deep levels to explain these strongly negative $\delta^{37}Cl$ values. This explanation remains problematic because no mineral that might sequester sufficient amounts of $^{37}Cl$-enriched chlorides to balance the $^{37}Cl$-depleted chlorides of the fluids, have been found (Barnes et al., 2006; Bonifacie et al., 2008; Sharp and Barnes, 2008; Wei et al., 2008b; Barnes and Cisneros 2012; Selverstone and Sharp, 2015, Bonifacie, 2017).

Ion filtration, sometimes referred as reverse osmosis, is a mechanism by which ionic species can be separated or mitigated when a liquid electrolyte is forced-flow through a charged membrane. In nature, it is speculated that clay-rich sediments could act as natural membrane, possibly resulting in modifying the chemical and the isotope compositions of porewater fluids circulating within sediment piles (Philipps and Bentley, 1987; Neuzil and Pearson, 2017). Philipps and Bentley have first suggested that such mechanism might have a role in producing the observed $^{37}Cl$-depletions in sediment pore waters because ion filtration might fractionate chlorine stable isotopes as negatively charged clay layers repel the negatively charged lighter $^{35}Cl$ ion slightly more than the $^{37}Cl$ ion. Consequently, $^{35}Cl$ becomes more enriched behind the clay layer relative to the direction of flow because of its higher ionic mobility (Figure 1). Yet, despite this potential isotopic effect, recent work by Neuzil and Pearson (2017), who simulated transport of NaCl across clay membrane, suggests that in natural conditions such mechanism would only produce modest salinity changes in pore fluids. This ion filtration process was invoked to explain the strongly $^{37}Cl$-depleted chlorides in fluids advected in mud volcanoes (Godon et al., 2004), in pore fluids of sediments (Bonifacie et al., 2007; Agrinier et al., 2019).

The purpose of the present study expands upon our previous work (Agrinier et al., 2019) and to explore the variability of pore fluids $\delta^{37}Cl$ in a wider variety of tectonic contexts (Table 1, supplementary material): i) oceanic basins, small and large, from the Atlantic and Pacific oceans and ii) rises from the Indian and the Atlantic oceans. These new data are here compared to previously published data on sedimentary piles from the Juan de Fuca Ridge Flank in the East of Pacific Ocean (Bonifacie et al., 2007); the foot of a continental shelf (Hesse et al., 2000) and the accretionary prisms from the West of the Pacific Ocean (Deyhle et al., 2003; Agrinier et al., 2019). This set of sedimentary piles encompasses a wide range of sedimentation styles and conditions ranging from high to very low rates of sedimentation (between 0.137m/ka and 0.003m/ka) and high to low rates of compaction (gradient of porosity between -0.16 %/m and -0.018 %/m). The sediment diagenesis temperature is low, less than 100°C in most of the cases (Table 1). The variations of $\delta^{37}Cl$ of the pore fluid chlorides are compared to those of other chemical parameters generally used as indicators of the sediment diagenesis : porosity, mineralogy, $Ca^{2+}$, $Mg^{2+}$ and oxygen stable isotopes of water, $\delta^{18}O$), which all change during the sediment ageing (Lawrence et al., 1975; Gieskes, 1976; Lawrence and Gieskes, 1981, Lawrence, 1991).

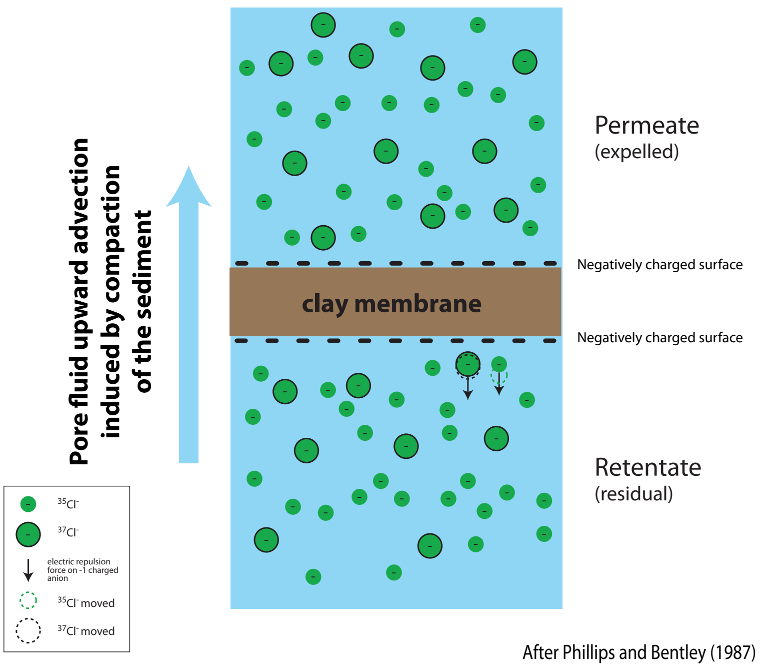


***Figure 1**: Schematic illustration of the Ion filtration process of chloride ions as described by Phillips and Bentley (1987), only chloride anions are drawn. In the flow of water towards the clay membrane, the movement of chloride ions is controlled by the negative electric potential created by the negatively charged surface of the clay particules and by the mobility of the chloride ions. Light chloride ions ($^{35}Cl$), more mobile than heavy*

*chloride ions ($^{37}Cl$), are repelled faster and further from the membrane. Therefore, they have a smaller probability to go through the membrane. This gives rise to chlorine isotope fractionation as light isotopes ($^{35}Cl$) are less transported through the clay membrane than heavy isotopes ($^{37}Cl$). Thus if the ion filtration fractionation is controlled by the density of negative charge on the mineral surface, it should be large for minerals with high density of negative charge on surface such as smectite, small or null for low density of negative charge on surface (kaolinite, carbonates) and medium for intermediate density of negative charge on surface (Illite, chlorite).*

*For hydrogen and oxygen isotope fractionation in water molecule between the retentate and the permeate, Phillips and Bentley (1987) suggest a different mechanism. The increased activity of heavy isotopic species (HDO and $H_2{}^{18}O$) in the membrane in comparison to that of $H_2{}^{16}O$, might possibly result in the increase of HDO and $H_2{}^{18}O$ in the retentate.*

*If these processes occurring during the filtration of porefluids in sedimentary piles hold true, deep pore fluids should be depleted in $^{37}Cl^-$, and enriched in HDO and $H_2{}^{18}O$ relative to seawater.*

Interestingly, these authors report that the water-sediment interactions are not sufficient to explain the decreases in $\delta^{18}O$ and the increases in $[Ca^{2+}]$ in the pore fluids. As a result of which they invoke fluxes of $^{16}O$-$Ca^{2+}$-enriched fluids from the basaltic basement into the overlying sediments. This suggests looking at other ways to explain these chemical changes in the pore fluids of the sediments. In particular the ion filtration that was suggested as a potential process, for modifying the $\delta^{18}O$ and ions concentrations of pore fluids (Phillips and Bentley, 1987; Haydon and Graf, 1986; Demir, 1988; Hanshaw and Coplen, 1973; Kharaka and Berry, 1973; and many other).

## II) Samples and Methods

We selected 226 pore fluids from 13 ODP-IODP sites (Figure 2, Table 1) with drill holes that deeply penetrated oceanic crust low temperature sediments. Selected sites are exclusively clay-rich sedimentary piles because we previously observed that clays are systematically present at the sites where the depletion of $^{37}Cl$ in in chlorides occurs (Agrinier et al., 2019). The reasons for this are twofold. First, the low permeability of clay-rich sediments ensures a good preservation of the indigenous pore fluids over the geological history of the sedimentary piles. Geological perturbations, such as the invasion of external fluids at high permeability levels, faults, rock sedimentary interfaces, have less impacts on the indigenous fluids. Second, clays play a role, via ion filtration process, in producing the $^{37}Cl$-depleted chlorides as suggested by Agrinier et al. (2019).

Table 1

| Sites | 645 | 646 | 647 | 757 | 758 | 997 | 1026 | 1028 | 1030 | 1150 | 1201 | C0011 | C0012 |
|---|---|---|---|---|---|---|---|---|---|---|---|---|---|
| Leg | 105 | | | 121 | | 164 | 168 | | | 186 | 195 | 322 & 333 | 322 |
| Sediment pile location | Proto oceanic basins Baffin Bay and Labrador Sea, North of Atlantic Ocean | | | Rifted fragment of oceanic plateaux Ninetyeast Ridge, Center of Indian Ocean | | Carolina Rise, Blake Ridge, west margin of Atlantic Ocean | Juan de Fuca Ridge Flank sediments, East of Pacific Ocean | | | Japan Trench, West of Pacific Ocean | Philippine Basin West of Pacific Ocean | Philippine plate in front of Nankai subduction zone, West of Pacific Ocean | |
| Age max (Ma) | 20 | 9 | 55 | 55 | 65 | 6 | 1.5 | 1.25 | 0.65 | 10 | 35 | 14 | 19 |
| Depth max (mbsf) | 1147 | 714 | 649 | 340 | 491 | 747 | 229 | 132 | 42 | 1168 | 505 | 850 | 529 |
| Simplified mineralogy of the sediments | Clay-rich, Carbonate < 20% | Clay-rich, Carbonate < 20% | Clay-rich, Carbonate < 20% | Cb-rich above 220 mbsf; ash and clay-rich below | Cb-rich above 350 mbsf; ash and clay-rich below | Clay-rich, Carbonate ≤ 25% | Clay-rich, Carbonate < 10% | | | Clay-rich, Carbonate < 15% | Clay-rich, Carbonate : rare | Clay-rich, Carbonate : rare | |
| Sedimentation rate m/ka[1] | 0.137 | 0.085 | 0.046 | 0.01 | 0.012 | 0.06 | 0.37 | 0.13 | 0.07 | 0.075 | 0.003 | 0.034 | 0.017 |
| Compaction rate[2] %/m | −0.13 | −0.062 | −0.21 | −0.15 | −0.07 | −0.041 | −0.17 | −0.18 | −0.14 | −0.018 | −0.16 | −0.055 | −0.092 |
| Maximum of temperature in sediment (°C) | <100 °C ? | <100 °C ? | <100 °C ? | <100 °C | <100 °C | <100 °C | <65 °C | <50 °C | <50 °C | <100 °C | <70 °C | ≤ 80 °C | <65 °C |
| Porosity model parameters[3] | (0.58; 400)[4] (0.57; 2200)[5] | (0.75; 1150) | (0.75; 300)[6] (0.83; 900)[7] | (0.74; 400) | (0.76; 900) | (0.72; 1700) | (0.71; 700) | (0.72; 300) | (0.77; 250) | (0.75; 4000) | (0.60; 900) | (0.76;1200) | (0.72; 745) |
| Reference | Srivastava et al., 1987a,b,c,d | | | Peirce et al., 1989a,b,c | | Paull et al., 2005a,b | Davis et al., 1997b,c | | | Sacks et al., 2005a,b | Richter et al., 2005 | Saito et al., 2010a,b, Henry et al., 2012a,b | |
| Minimum $\delta^{37}Cl$ | −5.22 | −4.78 | −4.61 | −2.31 | −2.18 | −3.68 | −1.9 | −2.1 | −0.8 | −1.11 | −3.2 | −8.52 | −6.8 |
| Depth of minimum $\delta^{37}Cl$ (mbsf) | 1021 | 714 | 369 | 190 | 491 | 747 | 229 | 132 | 42 | 875 | 505 | 779 | 292 |
| Age of minimum $\delta^{37}Cl$ (Ma) | >10.4 | <8.2 | <38.5 | ≈47.5 | >68 | ≥6 | ≥1.4 | ≈1.25 | ≥0.65 | 7 | >32.7 | 13.3 | 12.2 |
| $K^{35}$ | 1.00 | 1.00 | 1.00 | 0.94 | 0.94 | 1.15 | 0.97 | 0.97 | 0.97 | 1.6 | 0.82 | 1.02 | 0.985 |
| $K^{37}/K^{35}$ | 1.001–1.002 & 1.005–1.007 | 1.002–1.003 | 1.001–1.002 & 1.003–1.004 | 1.001–1.002 | 1.001–1.002 | 1.0025–1.0035 | 1.002–1.003 | 1.001–1.002 | 1.001–1.002 | 1.0005–1.00075 | 1.004–1.005 | 1.003–1.005 | 1.005–1.007 |
| Chemical data ref | Srivastava et al., 1987b,c,d | | | Peirce et al., 1989b,c | | Paull et al., 2005a,b | Davis et al., 1997b,c | | | Sacks et al., 2005a,b | Richter et al., 2005 | Saito et al., 2010a,b, Henry et al., 2012a,b | |
| $\delta^{18}O$ data ref | Zachos and Cederberg, 1989 | | | Lawrence, 1991 | | Hesse et al., 2000 | Mottl et al., 2000, Bonifacie et al., 2007 | | | Mora, 2005 | Komor and Mottl, 2006 | Destrigneville et al., 2016 | |
| $\delta^{37}Cl$ data ref | This work | | | This work | | Hesse et al., 2000 | Bonifacie et al., 2007, Bonifacie, 2005 | | | Deyhle et al., 2003 | This work | Agrinier et al, 2019 | |

[1] For the top 200 meters of the site.
[2] Mean gradient of porosity.
[3] Given as ($\Phi_0$; $\lambda$) for porosity model: $\Phi = \Phi_0 \exp(-z/\lambda)$ where z is the depth in meter, $\Phi$ is the porosity and $\lambda$ is the compaction length.
[4] For the 0–200 mbsf depth interval.
[5] For the 201–1200 mbsf depth interval.
[6] For the 0–100 mbsf depth interval.
[7] For the 101–800 mbsf depth interval. Cb: carbonate.

Using the pore fluids from ODP-IODP sites benefits from the policy of pore fluid sample preservation, storage and distribution since 1980 and the large scientific literature and data already published notably for chemical and isotope compositions ($Ca^{2+}$, $Mg^{2+}$ and $\delta^{18}O$). In this study, we use 127 pore fluids obtained from the ODP-IODP core repositories at Bremen and Kochi via the IODP sample and data request procedure (SaDR). They were analyzed for $\delta^{37}Cl$ during the course of this study. Additional 99 published $\delta^{37}Cl$ data are also considered in this study (Hesse et al., 2000; Deyhle et al., 2003; Bonifacie, 2005; Bonifacie et al., 2007 and Agrinier et al, 2019).

During these ODP-IODP legs, immediately after recovery, pore fluids were extracted from the sediment by squeezing core sections (Manheim, 1966), filtered through 0.45 µm and then stored in glass vials. The squeezing on board the ship was made at very low pressure (< 170 MPa), which ensured that no or very small chemical and isotope fractionations in the extracted pore fluids occurred (Coleman et al., 2001; Mazurek et al., 2015; Bonifacie et al., 2007). Major element concentrations in pore fluids were determined by HPLC using the methods of Gieskes (1974). Concentration in major elements Ca, Mg, Na were compiled from previous publications: Srivastava et al. (1987b, c and d); Peirce et al. (1989b and c); Davis et al. (1997b and c); Saito et al. (2010a and b); and Henry et al. (2012 a and b). The $\delta^{18}O$ values of the pore fluids were compiled from Zachos and Cederberg (1989), Lawrence (1991), Mottl et al. (2000), Mora (2005), Komor and Mottl (2006) and Destrigneville et al. (2016) using the $CO_2$-$H_2O$ equilibration method of Epstein and Mayeda (1953). Precision is better than 0.1 ‰.

The $\delta^{37}Cl$ of the pore fluids for Sites 1026, 1028 and 1030 were reported by Bonifacie et al. (2007) and for Sites C0011 and C0012 by Agrinier et al. (2019) using the AgCl-$CH_3Cl$ method routinely used at IPGP (Kaufmann, 1984; Eggenkamp, 1994 and Godon, 2004). The external reproducibility of the seawater standard was 0.09 ‰ (1σ, n = 10) in Bonifacie et al (2007), 0.04 ‰ (1σ, n = 18) in Agrinier et al (2019). The $\delta^{37}Cl$ of the pore fluids for Site 997 (Hesse et al., 2000) and for Site 1150 (Deyhle et al., 2003) were measured at the University of Waterloo, Canada, using the AgCl-$CH_3Cl$ method. Precision on reported $\delta^{37}Cl$ are 0.15 ‰ (1 σ).

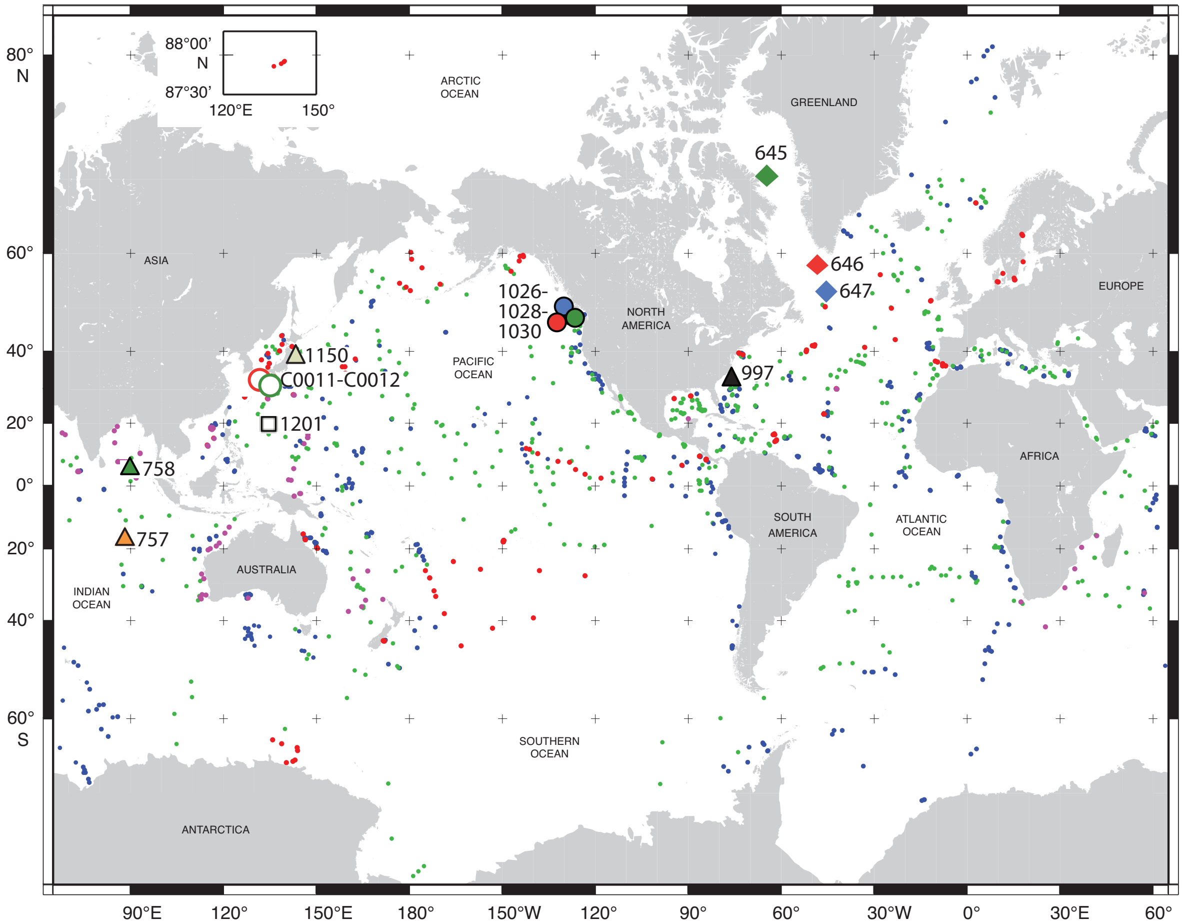


***Figure 2** : ODP-IODP Site sedimentary pile pore fluids studied in this work (large black dots). Sites 645, 646 and 647 are in sedimentary basins with decreasing influence of continental influxes in the Atlantic Ocean. Sites 1150, C0011 and C0012 are located in front of subduction zones offshore Japan, West of Pacific Ocean. Site 1201 is in the northern West Philippine Basin, West of Pacific Ocean. Sites 757 and 758 are on ocean plateaux in the center of Indian Ocean. Site 997 is at the foot of the continental margin of west Atlantic Ocean. Sites 1026, 1028 and 1030 are on the east flank of the Juan de Fuca Ridge, East of Pacific Ocean. Drill site map from ODP-IODP : Green dots are DSDP Legs 1-96. Blue dots are ODP Legs 100-210. Red dots are IODP Expeditions 301-348. Purple dots are IODP Expeditions 349-371.*

For the present study, 127 pore fluids from the Sites 645, 646, 647, 757, 758 and 1201 were measured for $\delta^{37}Cl$ of chlorides at IPGP using the AgCl-$CH_3Cl$ method and dual-inlet gas source mass spectrometer (Delta plus XP or Delta V from ThermoFisher), as originally described in Eggenkamp (1994) and adapted at Institut de Physique du Globe de Paris as described in Godon et al. (2004). Over the course of the present study, the external reproducibility of the seawater standard was excellent (± 0.025 ‰, 1σ, n = 48). Eighteen pore fluids were measured twice. The mean absolute $\delta^{37}Cl$ difference value between duplicate measurements was 0.022 ± 0.018 ‰.

The many decade long–term storage of the pore fluids since their shipboard sampling has been realized without loss in quality for chlorine isotopes of chlorides as suggested by the strong correlations between the $\delta^{18}O$ data (measured by others: Zachos and Cederberg, in 1989, Lawrence in 1991, Mottl et al. in 2000, Mora in 2005, Komor and Mottl, in 2006) and the $\delta^{37}Cl$ data (measured by us in 2007, 2017 and 2019 and taken from literature), (see below Figure 6 and Figure sup 2). Alterations of chlorine isotopes of chlorides during the handling, storage, shipment, such as contamination, adsorption onto the surface of containers, drying of the pore fluids would certainly have affected the quality of these $\delta^{37}Cl$- $\delta^{18}O$ correlations.

**III) Depth profiles of chemical and isotopic compositions**

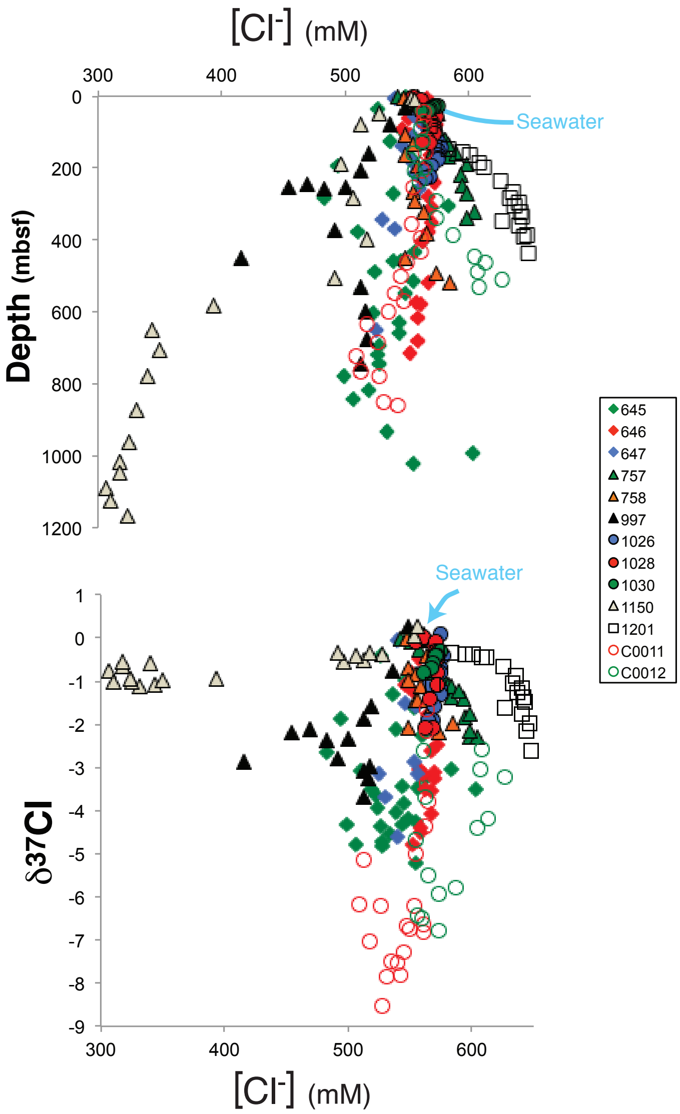


***Figure 3**: Geochemical characters of chlorides of the pore fluids (data from Table of supplementary material): **Top** : Depth profiles of chloride concentrations, [Cl-]. **bottom**: chlorine isotope compositions of chlorides ($\delta^{37}Cl$) vs. [Cl-]. Only [Cl-] of Sedimentary piles 645, 757, 997, 1150, 1201 and C0012 deviate significantly from the chloride seawater concentration (≈ 558 mM). In the other sedimentary piles (646, 647, 1026, 1028, 1030 and C0011), [Cl-] stays, within a few percent, close to the seawater chloride concentration. ($\delta^{37}Cl$ of seawater chlorides from Godon et al., 2004b).*

Chemical and isotope compositions of the pore fluids are given in the Table of the supplementary material. Figures 3 and 4 display depth profiles of the pore fluid chlorine isotopic compositions, $\delta^{37}Cl$, and concentrations, $[Cl^-]$.

While the chloride concentration is similar to that of seawater at the top of all the sedimentary piles (≈ 558mM), the chloride concentration profiles evolve differently at depth (Figure 3). In sedimentary piles 757, 1201 and C0012, $[Cl^-]$ increases with depth (≤ 16%) while it decreases with depth in sedimentary piles 645, 997, 1150 and C0011 (≤ 25%), with a significant decrease of 45% in site 1150). In the other sedimentary piles, $[Cl^-]$ stays roughly close to the seawater concentration (±15%).

In Figure 4, all the investigated sedimentary piles systematically describe a decrease in $\delta^{37}Cl$, from seawater value (= 0 ‰) at the top of the sedimentary pile to very negative minima (lowest $\delta^{37}Cl$ values is -8.52 ‰ at C0011) which are often found at the greatest depth. Positive $\delta^{37}Cl$ values are extremely rare, only 3 values out of 226 data and are weakly $^{37}Cl$-enriched relative to seawater (maximum $\delta^{37}Cl$ value is + 0.26 ‰). In general, the decrease in $\delta^{37}Cl$ is larger than 5 ‰ for the thick sedimentary piles (645, 646, 647, 1150, C0011 and C0012, that sampled pore fluids deeper than 400 mbsf and small (≤ 2 ‰) for thiner sedimentary piles (757, 1026, 1028, 1030, 1201). Sedimentary pile 1150 with pore fluids as deep as 1150 mbsf is an anomaly as the maximum depletion in $\delta^{37}Cl$ is only -1.1 ‰ at 875 mbsf.

Near the seafloor, the $\delta^{37}Cl$ profiles are rather smooth whatever the complexity of the lithostratigraphy of the sedimentary piles. However, in sedimentary pile 647, the $\delta^{37}Cl$ profile present discontinuities associated with porosity jumps and the sedimentary hiatuses, but such discontinuity does not show up for sedimentary pile 758, which also has porosity jumps and a sedimentary hiatus.

Generally, the gradients of the $\delta^{37}Cl$ versus depth are about the same, about ≈ -0.009 ± 0.002 ‰.$m^{-1}$ except for Sedimentary pile 1150, which has a much smaller gradient, -0.0025 ‰.$m^{-1}$. In all the sedimentary piles, when depth is deeper than 300-400 mbsf, the $\delta^{37}Cl$ profiles become noisy and their gradients flatten and eventually reversed (Sites 647, C0011 & C0012*)*. The noise in the $\delta^{37}Cl$ profiles increases with depth. This can be interpreted as the decrease in the influence of the seawater chlorides into the sedimentary pile. The damping of the gradients suggests that there are minima to the depletion of $^{37}Cl$, which are different from one pile to another.

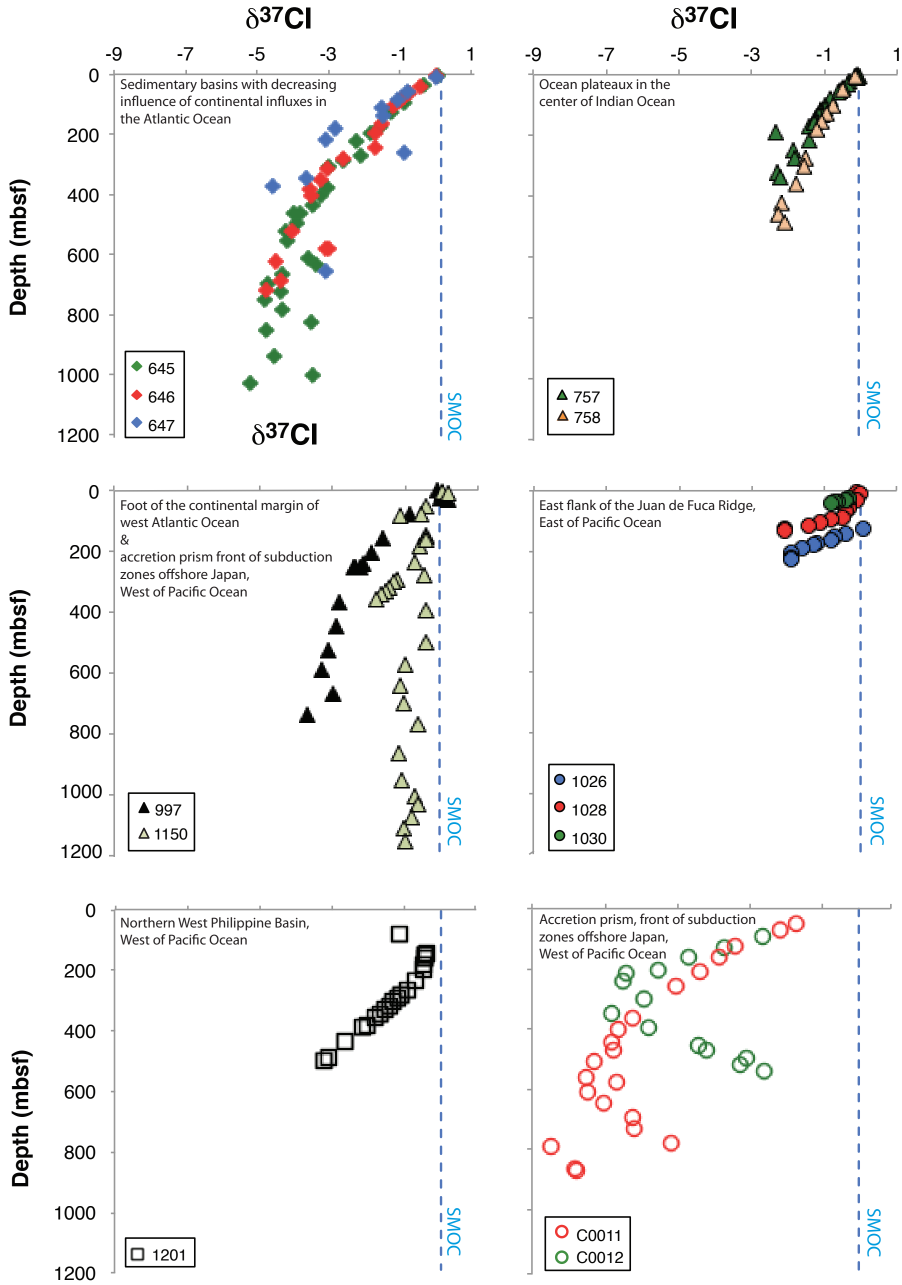


***Figure 4** : Depth profiles of the chlorine stable isotope ratio of chlorides ($\delta^{37}Cl$) of the pore fluids discussed in this work (data from data from Table of supplementary material). Notewortingly amongst the 226 samples analysed here, all but 3 $\delta^{37}Cl$ data, are negative, that is depleted in $^{37}Cl$ relative to seawater (SMOC, the standard mean ocean chloride, is a very good representation of the seawater whose $\delta^{37}Cl$ variability was measured smaller than ± 0.08 ‰ on 24 seawater samples collected worldwide (Godon et al., 2004b). mbsf : meter below seafloor.*

Sedimentary pile 1150 $\delta^{37}Cl$ minimum is -1.1 ‰; minima of 645, 646, 647 and 997 are -5 ‰, minimum of C0012 is -7 ‰ and that of C0011 is -8.5 ‰. Similar dampings of the gradient of the $\delta^{37}Cl$ and minima are common in clay-rich sedimentary piles. They are observed in sedimentary piles of Sites 808, 1173 and 1174 where gradients are larger, about -0.022 ± 0.01 ‰.m$^{-1}$ and minima are -8, -6 and -6 ‰ respectively, (data from Wei et al. (2008), not reported here). Sites 757, 1026, 1028, 1030 and 1201 do not show constant gradients, and consequently have no local minima probably because the sedimentary pile was not drilled deep enough (only 160 and 360 mbsf for Sedimentary piles 757 and 1201, respectively) and/or because the sedimentary pile was not mature in term of thickness or age (1026-1028-1030, ages ≤ 1.5 Ma) to reach a limit of $^{37}$Cl-depletion. The minima are systematically located in clay-rich depth intervals with low permeability, 800-1000 mbsf in 645 (Thiebault et al. 1989); 700-800 mbsf in 646 (Cremer et al. 1989); 400-500 mbsf in 647 (Nielsen et al., 1989); 700-800 mbsf in 997 (Paull et al., 1996); 700-800 mbsf in C0011 and 300-400 mbsf in C0012 (Underwood et al, 2010); Henry et al., 2012a,b); 900-1000 mbsf in 808 (Mikada et al., 2002a); 600-650 mbsf in 1173 (Mikada et al., 2002b); 1000-1050 mbsf in 1174, (Moore et al., 2001)). As suggested by Agrinier et al. (2019), these low-permeability conditions have contributed to create and to preserve $^{37}$Cl-depleted chlorides over longer periods up to 50 Ma in Sedimentary piles 646 and 757.

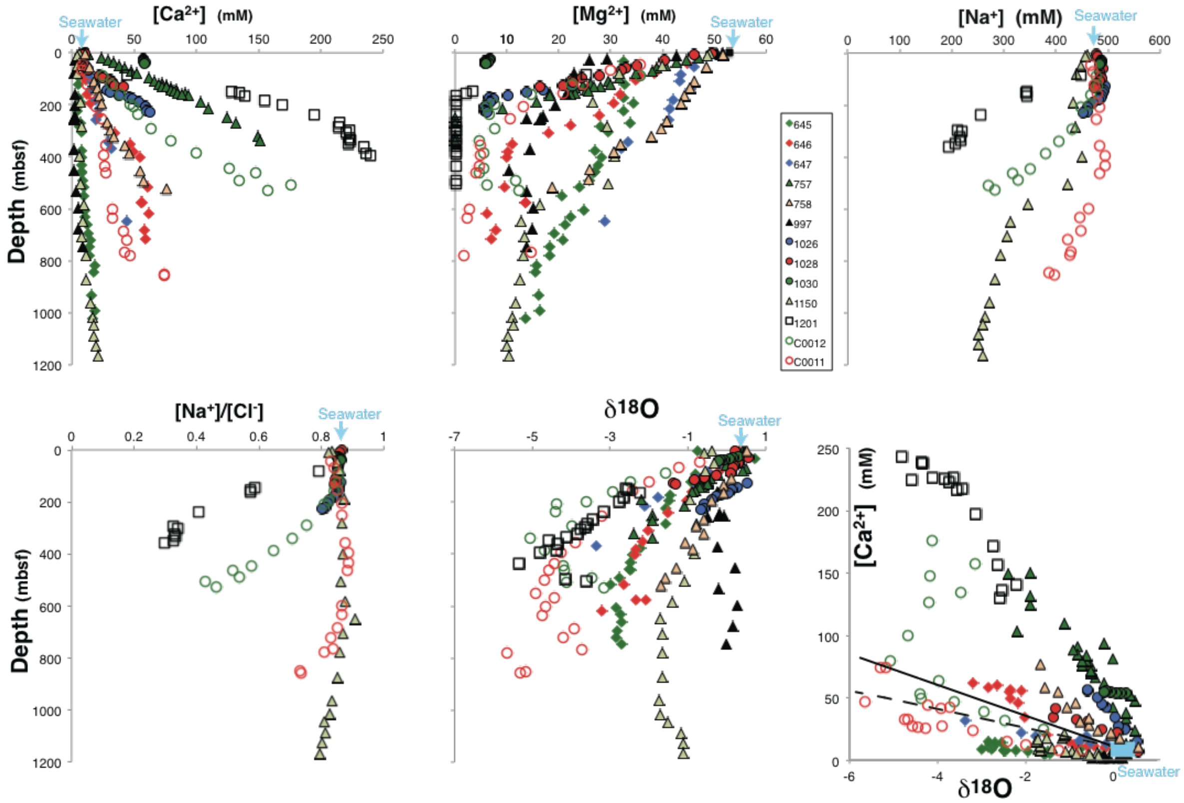


***Figure 5**: The pore fluid concentrations of $Ca^{2+}$(upper left), $Mg^{2+}$(upper center), $Na^{+}$(upper right), $[Na^{+}]/[Cl^{-}]$ ratio (bottom left), $\delta^{18}O$(bottom center) depth profiles and the $\delta^{18}O$ vs. $[Ca^{2+}]$ graph (bottom right). On the $\delta^{18}O$ vs. $[Ca^{2+}]$ graph, the lines of Lawrence and Gieskes (1981) are reported. They are the mean gradient (-0.13‰ per mM, dash line) and the preferred gradient (-0.08‰ per mM, solid line) of a vast set of oceanic crust pore fluids*

All these sedimentary piles have pore fluids that display increase in $[Ca^{2+}]$, decreases in $[Mg^{2+}]$, $[Na^{+}]$ contents and $\delta^{18}O$ values with depth (Figure 5). These geochemical changes are common features in oceanic sediment pore fluids (Lawrence et al., 1975, 1979; Gieskes et al., 1976; Lawrence and Gieskes, 1981; Gieskes and Lawrence, 1981).

$Ca^{2+}$ increases by a factor 1 to 23 relative to seawater content (10 mM) depending the sedimentary pile. Each sedimentary pile has a specific and well-defined gradient of increase (Figure 5) spanning from very small (≤ 0.05 mM.m$^{-1}$ in 997, 645 and 1150) to very large values (> 0.5 mM.m$^{-1}$ in 1201 and 757).

$Mg^{2+}$ decreases from seawater value (54 mM) to values as low as zero. The gradient of decrease is large for Sedimentary piles 1030 and 1201, which have lost almost all the $Mg^{2+}$ within the first 200 mbsf. Gradients are medium for most of the sedimentary piles and small for 645, 647 and 758 (less than -0.05 mM.m$^{-1}$).

[$Na^+$] data are available only for 7 sedimentary piles (1026, 1028, 1030, 1150, 1201, C0011 & C0012). The [$Na^+$] gradients of decrease are generally small or null at the top of the sedimentary piles then, increase eventually at depths deeper than 200 mbsf (1201, C0012, 1150). The change in [$Na^+$] offsets the changes in [$Ca^{2+}$] and in [$Mg^{2+}$].

For $\delta^{18}O$, the gradient of decrease is large for Sedimentary piles C0012, 1201 and C0011 (-0.02 ‰.m$^{-1}$), medium for most of the sites and small or null for 1150 and 997 (< -0.005 ‰.m$^{-1}$) (Figure 5, subplane of $\delta^{18}O$ vs. depth). As shown in Lawrence and Gieskes (1981) for a large number of sedimentary piles, each sedimentary pile has a specific $\delta^{18}O$ - [$Ca^{2+}$] relationship.

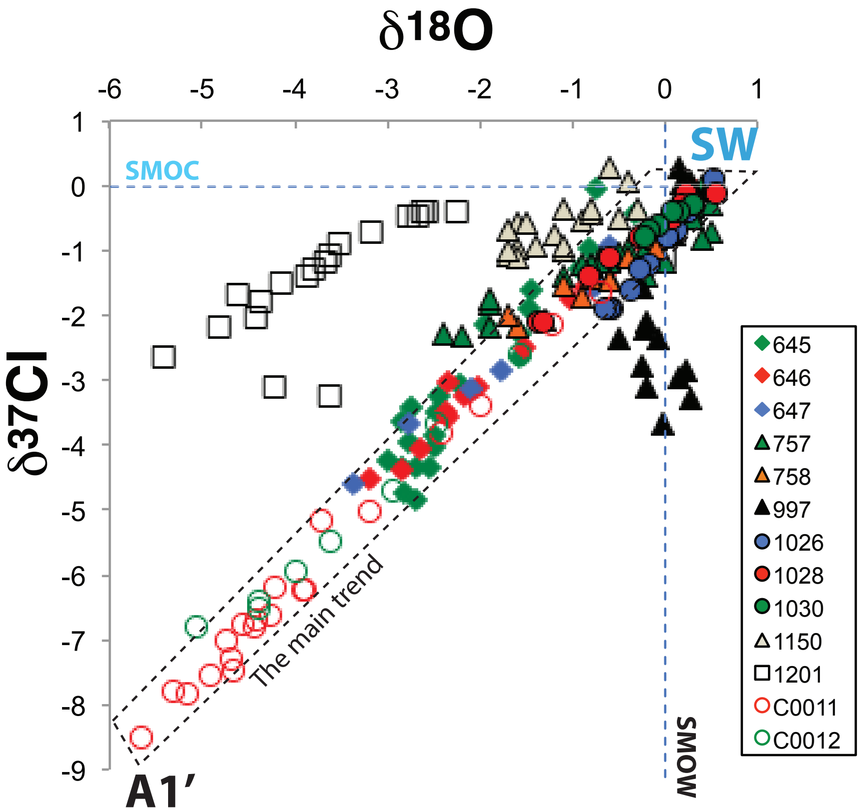


***Figure 6*** *: the $\delta^{37}Cl$ and $\delta^{18}O$ data of the pore fluids discussed in this work. Most of the data plot on « The main trend » that links the SW extremum, slightly $^{18}O$-enriched (by about +0.5 ‰) in comparison to SMOW, to the A1' extremum (sample 322-C0011B 55R-2), strongly depleted in $^{18}O$ and $^{37}Cl$ (of Agrinier et al., 2019). The « main trend », $\delta^{37}Cl \approx 1.37 * \delta^{18}O -0.42$, may be explained by variable contributions of the process that created the*

*extremum A1'. Note that the $\delta^{37}Cl$– $\delta^{18}O$ trends of Sedimentary piles 1150 and 1201 are shifted above « The main trend».*

The most striking features emerging from the pore fluid data are the $\delta^{18}O$-$\delta^{37}Cl$ linear correlations illustrated in Figure 6. There, it appears that pore fluids, from 9 of the 13 investigated sedimentary piles (646, 647, 757, 758, 1026, 1028, 1030, C0011 & C0012) plot on a main trend between the seawater extremum (SW: $\delta^{18}O$ = +0.5, $\delta^{37}Cl$ = 0) and the A1' extremum ($\delta^{18}O$ = -5.66, $\delta^{37}Cl$ = -8.52, Sample 322-C0011B 55R-2) of C0011 as defined in Agrinier et al. (2019). This linear correlation has a slope of ca. 1.4 (correlation coefficient is 0.98 with n = 126). Sedimentary piles 645, 1150 and 1201 data define three other linear trends above the main trend. Sedimentary pile 1026 linear trend has a much steeper slope, of ca. 2.2, than that of the main trend. The sedimentary pile 997 is the only one to not show a $\delta^{18}O$-$\delta^{37}Cl$ relationship. However, it should be noticed that no variation of the variation of the $\delta^{18}O$ is observed with depth in this pile. Overall, in 12 of the 13 studied sedimentary piles, strong linear correlations between the $\delta^{18}O$ of water and the $\delta^{37}Cl$ of the pore fluids are observed (Table 2).

*Table 2 : Slope and intercept of the $\delta^{37}Cl$–$\delta^{18}O$ relationship for each site ($\delta^{37}Cl$ = slope * $\delta^{18}O$ + intercept), data displayed on Figure 6. Sedimentary pile 997 is not reported because it does not display a clear $\delta^{37}Cl$–$\delta^{18}O$ linear relationship($r \approx 0.42$, n=16). The main trend is composed of the pore fluids from sedimentary piles 646, 647, 757, 758, 1028, 1030, C0011 and C0012)*

| Site | 645 | 646 | 647 | 757 | 758 | 1026 | 1028 | 1030 | 1150 | 1201 | C0011 | C0012 | Main trend |
|---|---|---|---|---|---|---|---|---|---|---|---|---|---|
| Number of data | 23 | 18 | 10 | 30 | 13 | 13 | 11 | 6 | 19 | 17 | 20 | 8 | 147 |
| Correlation coefficient | 0.951 | 0.988 | 0.994 | 0.926 | 0.964 | 0.893 | 0.990 | 0.974 | 0.746 | 0.980 | 0.994 | 0.989 | 0.980 |
| Slope | 1.837 | 1.278 | 1.229 | 0.784 | 0.938 | 2.244 | 1.123 | 1.000 | 0.782 | 0.677 | 1.427 | 1.306 | 1.373 |
| *Sigma on slope* | *0.054* | *0.031* | *0.039* | *0.024* | *0.051* | *0.184* | *0.061* | *0.270* | *0.028* | *0.038* | *0.027* | *0.048* | *0.079* |
| Intercept | 0.825 | -0.484 | -0.501 | -0.616 | -0.720 | -0.688 | -0.545 | -0.547 | 1.678 | 1.322 | -0.433 | -0.628 | -0.424 |
| *Sigma on intercept* | *0.120* | *0.056* | *0.065* | *0.022* | *0.046* | *0.066* | *0.042* | *0.048* | *0.105* | *0.136* | *0.109* | *0.177* | *0.0168* |
| $r_{error}$* | 0.941 | 0.807 | 0.745 | 0.577 | 0.735 | 0.206 | 0.381 | -0.075 | 0.974 | 0.978 | 0.948 | 0.958 | 0.682 |
| Fisher's $p(H_0)$ value** | $< 8\ 10^{-18}$ | $< 6\ 10^{-17}$ | $< 6\ 10^{-8}$ | $< 8\ 10^{-23}$ | $< 2\ 10^{-8}$ | $< 4\ 10^{-6}$ | $< 2\ 10^{-8}$ | $< 2\ 10^{-2}$ | $< 3\ 10^{-7}$ | $< 3\ 10^{-14}$ | $< 4\ 10^{-22}$ | $< 7\ 10^{-7}$ | $< 10^{-200}$ |

*the correlation coefficient between the error on slope and the error on intercept. Slope, intercept and errors were calculated using algorithm of Minster et al. (1978). **The probability of obtaining a $\delta^{37}Cl$–$\delta^{18}O$ relationship equal to or more extreme than the one observed considering the null hypothesis is true.

To compare the $\delta^{37}Cl$–$\delta^{18}O$ trends, we display the error ellipses (uncertainty domain at the 86% probability level) for the slope and the intercept of each $\delta^{37}Cl$–$\delta^{18}O$ lines (Table 2 and Figure 7). Ellipses of sedimentary piles that plot on the main trend overlap each other suggesting that these sedimentary piles display the very similar linear relationship.

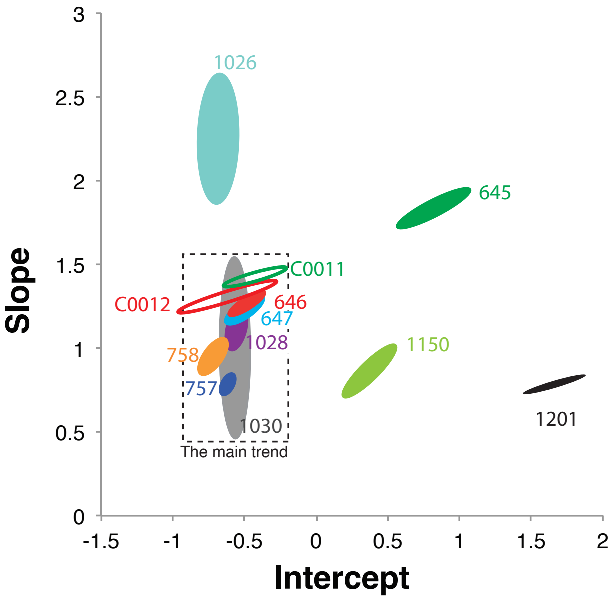


***Figure 7*** *: Error ellipses at 86% probability level for the slope and intercept of the δ³⁷Cl–δ¹⁸O relationships displayed on Figure 5. Dashed rectangle delimits the members of the « main trend» between the SW and A1' endmembers of Figure 5. No ellipse is shown for Sedimentary pile 997 because it does not display a clear δ³⁷Cl–δ¹⁸O linear relationship (r = 0.42).*

Nine sedimentary piles (646, 647, 757, 758, 1026, 1028, 1030, C0011 and C0012) have linear trends with intercept values concentrated closely to -0.57 ± 0.10. This means that for $\delta^{37}Cl$ = 0 ‰ (the seawater value) the interpoled $\delta^{18}O$ value is 0.50 ± 0.18 ‰ (1 σ). This interval is in agreement with that of the seawater's $\delta^{18}O$, ranging from 0.1 to 0.6 ‰, over the last 5 My (Cramer et al., 2011). The three other sites: 645 (= 0.82), 1150 (= 0.37) and 1201 (= 1.32) have intercept values significantly higher than -0.5. The slopes are in the 0.5-1.5 interval mostly.

## IV) Discussion

Remarkably, all the pore fluids but those of Sedimentary pile 997 have similar geochemical relationships between their major components: a marked enrichment in $Ca^{2+}$ and marked depletions in $Mg^{2+}$, $^{18}O$, $^{37}Cl$ in comparison with the seawater concentrations. Chlorinity remains close to that of seawater (within ± 20 %) but in Sedimentary piles 1150 (decreased by 45 %) and 1201 (increased by 25%). These geochemical characters are occurring in all the clay-rich sedimentary piles whatever the tectonic context: subduction zone accretionary prisms (1150, C0011, C0012), ridge flanks (1026, 1028, 1030), sedimentary basins (645, 646, 647), oceanic plateaux and basins (757, 758, 1201).

### *IV.1) chlorine isotope composition of chlorides*

The systematic depletion of $^{37}Cl$ in chlorides of all the pore fluids in comparison to seawater is intriguing as chlorides are unreactive which causes them to remain in solution with very little incorporation into minerals at low temperature. Clay minerals can store less than 100 ppm Cl (Kendrick, 2018), which is much lower than the pore fluids (≈ 19000 ppm Cl). Hence clays cannot compensate for the missing $^{37}Cl$ of pore fluid chloride without calling for unrealistic $\delta^{37}$Cl values (≥ 200 ‰) of chloride stored within clays. Therefore the missing $^{37}$Cl cannot be sequestrated in mineral structure or adsorbed on their surfaces. Bonifacie et al. (2007) investigated whether residual chlorides, either in the form of salts formed by desiccation or adsorbed on mineral surfaces, in the cores and pore fluid chlorides obtained by squeezing have different values $\delta^{37}$Cl. They were shown to be identically $^{37}$Cl-depleted. In consequence, the conservation of chlorine isotopes leads to deduce that the process creating the $^{37}$Cl-depleted chloride pore fluids expelled out of the sediment $^{37}$Cl-enriched chloride fluids or that $^{37}$Cl-depleted chloride fluids have invaded the sediments. Thus, the geochemical properties of chlorides suggests that processes that specifically involving the fluids should be examined. In the following part, we address the physical processes occurring in pore fluids, such as mixing of fluid, diffusion and gravity, ion filtration, which are known to change the chlorine isotope ratios of chlorides.

*IV.1.1 Mixing by advection of $^{37}$Cl-depleted fluid into the sedimentary piles.* This process was proposed for subduction zone accretionary sedimentary prisms (Ransom et al., 1995; Spivack et al., 2002 and Wei et al., 2008). Indeed, invasion of exogenous deep fluids into the sedimentary piles could explain the observed $^{37}$Cl, $^{18}$O, $Mg^{2+}$ and $Ca^{2+}$ changes. It would require the injected fluids to be depleted in $^{37}$Cl, $^{18}$O and $Mg^{2+}$ and enriched in $Ca^{2+}$ such as the A1' extremum (i.e. sample 322-C0011B 55R-2 with $\delta^{37}$Cl = -8.52 ‰, $\delta^{18}$O = -5.66 ‰, $Mg^{2+}$ ≤ 1.7 mM and [$Ca^{2+}$] ≥ 47 mM, Table 2 and Figure 6). From a compilation of porefluid in many sedimentary piles, Lawrence and coworkers proposed such contributions of $^{18}$O-$Ca^{2+}$ modified deep fluids coming from the basalts of Layer II of the oceanic crust to explain the depletions in $^{18}$O and the enrichments in $Ca^{2+}$ which cannot be entirely explained by water-rock exchanges in the sediment (Lawrence et al., 1975, 1979; Gieskes et al., 1976; Lawrence and Gieskes, 1981; Gieskes and Lawrence, 1981). Then, in the sedimentary piles studied here, where altered basalts are constituting the basement, the process of advection of deep fluid upwards may contribute to explain the $^{18}$O-$Ca^{2+}$ data. However Bonifacie et al. (2007) measured at the bottom of Sedimentary pile 1026, fluids that advect from the basaltic basement. They measure chlorinity and $\delta^{37}$Cl close to those of seawater (551 mM and -0.28 ‰), thus isotopically distinctfrom the $^{37}$Cl-depleted chloride measured in the local pore fluids (of ca. -1.9 ‰). Similar contrasts occur in Sedimentary Piles C0011 and C0012, where the near the basaltic basement pore fluids, have less marked depletions in $^{37}$Cl (respectively -5.16 ‰ & -2.58 ‰) than most $^{37}$Cl-depleted pore fluids (respectively -8.5 ‰ and -5.7 ‰). Thus for these three cases, the fluids escaping from the basaltic basements of the oceanic crust have are not impoverished enough in $^{37}$Cl to explain the observed $^{37}$Cl-depletions in the sediment pore fluids. Moreover, to explain the depletions in $^{37}$Cl of the pore fluids of the sediments, the deep fluid upward advection would require very large fluxes (≥ $10^{-5}$ Mole of $Cl^{-}.m^{2}$.year) in order to overprint the pristine seawater-like isotopic composition ($\delta^{37}$Cl = 0 ‰) of the chloride. Such large fluxes are hardly compatible with a typical characteristic of clay-rich sediments (including those studied here), which is their extremely low permeabilities.

Instead, as the $^{37}$Cl-depletion of chlorides is a common character of all the studied sedimentary piles, we suggest that the process process responsible for the observed depletions in $^{37}$Cl must be specific to the sedimentary piles.

*IV.1.2) Diffusion and Gravity :* for large chloride concentration gradients, aqueous diffusion of chlorides produces $^{37}$Cl-depletions of the low concentration side (Eggenkamp et al., 1994; Hendry et al., 2000; Lavastre et al., 2005; Eggenkamp and

Coleman, 2009, Giunta 2015). Current knowledge on chlorine isotope fractionation factors for diffusion (1.00128 – 1.00192, Eggenkamp and Coleman, 2009) and on chloride diffusion coefficients (1 to 3 $10^{-9}$ $m^2/s$, Eggenkamp and Coleman, 2009; Li and Gregory, 1974, Giunta 2015) show that it is not possible to generate a $^{37}Cl$-depletion larger than 1 ‰, with chloride concentrations in the 100-1000 mM range within a diffusion time smaller than 100 Ma. $\delta^{37}Cl$ decreases larger than 3 ‰ are obtained only for chloride concentrations downstream lower than 10 mM i.e. unrealistic conditions in the oceanic sediment pore fluids. Thus diffusion of chlorides cannot be the process that generates the observed $^{37}Cl$-depletions in the oceanic crust pore fluids. Recently, Giunta et al. (2017a) have also proposed that in vertical water profile, a dynamic equilibrium between diffusion and gravitational settling would result in typical $\delta^{37}Cl$ increase with depth – which is the opposite of what is observed in the sedimentary piles studied here.

*IV.1.3) Ion filtration induced by compaction:* As shown in the figure of the supplementary material (Figure sup. 1), there are good similarities in shape between porosity and $\delta^{37}Cl$ profiles at most of sedimentary piles. This suggests that the compaction, which drives the evolution of porosity in sedimentary piles, may have some influence on the chlorine isotope compositions of chlorides. Since compaction reduces the porosity, pore fluids are forced to flow through solid part (mainly clays) of the sediment (Berner, 1981; Hutchinson, 1985). This creates the filtration of dissolved ions by clays. As suggested by Philipps and Bentley (1982), it could produce chlorine isotope fractionation because the mobility of $^{37}Cl^-$ is smaller than that of $^{35}Cl^-$ (see Figure 1).

The intensity of the compaction-induced ion filtration can be assessed via $F_{fluid}$ :

$$F_{fluid} = 1 - \left[\frac{\phi_z}{\Phi_0}\frac{(1-\Phi_0)}{(1-\phi_z)}\right] \qquad (1)$$

which gives the proportion of initial fluid lost by the sediment at depth z due to compaction ($\Phi_0$, is porosity at depth z=0, and $\Phi_z$, that at depth z, Agrinier et al., 2019). Analogously, at depth z, $F_{chloride}$,

$$F_{Chloride} = 1 - \left[\frac{\phi_z}{\Phi_0}\frac{(1-\Phi_0)}{(1-\phi_z)}\ \frac{[Cl^-]_z}{[Cl^-]_{seawater}}\right] \qquad (2)$$

the proportion of initial chlorides lost by the sediment is obtained by writing that the change of the quantity of chloride for a given mass of solid ($[Cl^-]_{seawater}$ and $[Cl^-]_z$ are chlorinities at the seawater-sediment interface and at depth z, respectively). In fact, $F_{chloride}$ measures not only the effect of the compaction but also includes the effects of diagenetic processes that changes chlorinity via water consumption and production. $F_{chloride}$ and $F_{fluid}$ are close if $[Cl^-]_z$ is close to $[Cl^-]_{seawater}$. Getting a value $\Phi_0$ from the present day porosity profile is not straightforward as the style of sedimentation and burial history may have changed with time and consequently sediment layers could have compacted at different rates with respect to overburden pressure. Porosity profiles that fit well the steady-state compaction equation ($\Phi_z = \Phi_0 \exp(-z/\lambda)$, where z is the depth and $\lambda$, the compaction length; Athy, 1930) are those of Sedimentary piles 646, 757, 758, 997, 1150, C0011 and C0012. Their $\Phi_0$ values can be determined and their $F_{fluid}$ and $F_{chloride}$ calculated.

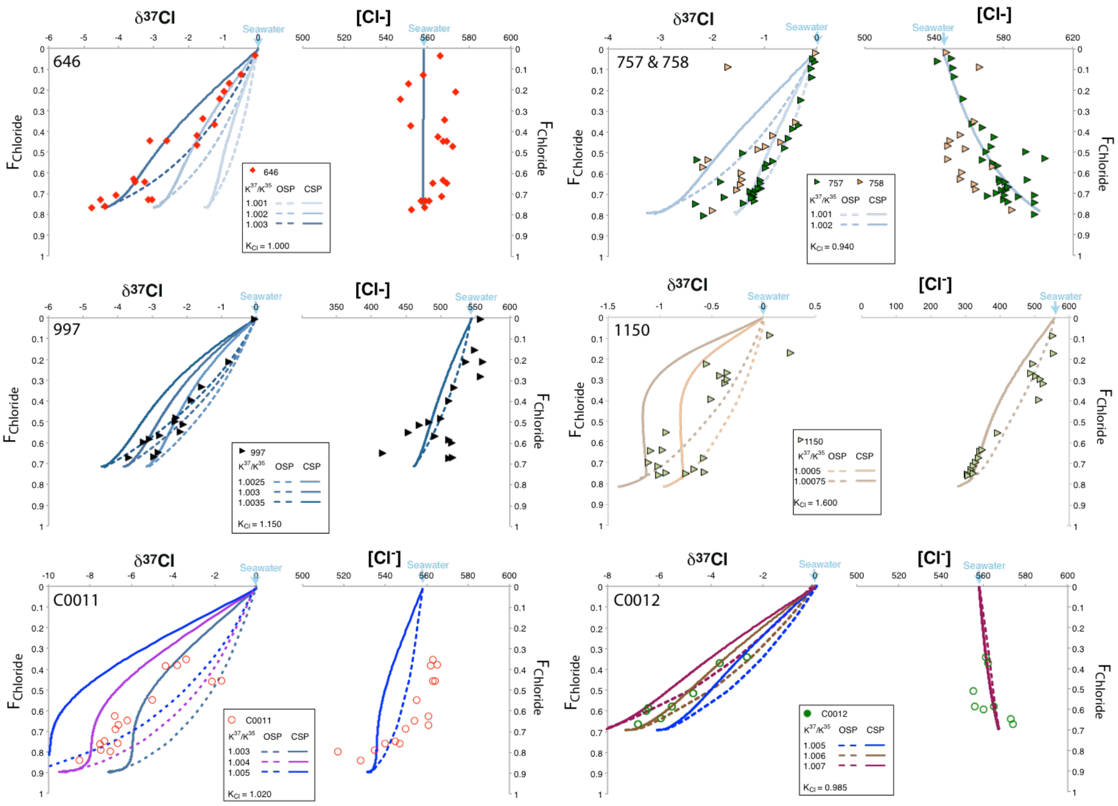


***Figure 8**: Comparison of Sedimentary piles 646, 757, 758, 997, 1150, C0011 and C0012 pore fluid chloride data with curves of the 1D model of compaction- induced ion filtration of pore fluids of Agrinier et al. (2019). $F_{chloride}$ is the proportion of initial pore fluid chlorides lost by the reduction of porosity induced by sediment compaction (note Y-axis is inverted). CSP: closed sedimentary pile (expelled fluid migrates vertically through the pile); OSP: open sedimentary pile (expelled fluid migrates out of the pile through fractures). The chloride concentration curves are for $K_{Cl}$ values (= $[Cl_{expelled\ fluid}]/[Cl_{residual\ fluid}]$, the partition coefficient of chloride between the expelled and the residual fluids), which are ranging between 0.94 and 1.60. $K^{35}$ (= $^{35}Cl_{expelled\ fluid}/^{35}Cl_{residual\ fluid}$) is that for $^{35}Cl$ and $K^{37}$ that for $^{37}Cl$. The $\delta^{37}Cl$ curves are for the chlorine isotope fractionation factor, $\alpha^{37}Cl/^{35}Cl_{(expelled\ fluid-residual\ fluid)}$ = $K^{37}/K^{35}$, ranging from 1.008 to 1.001. (nb. The $K^{37}$ values are varied within a few $10^{-3}$ above the $K^{35}$ values and therefore $K_{Cl} \approx K^{35} \approx K^{37}$, not necessarily equal to 1). These values of K's are mandatory to reproduce both the $\delta^{37}Cl$ and the chloride concentrations of the pore fluids.*

These sites, with « regular » porosity profile, define trends in the $[Cl^-]$ and $\delta^{37}Cl$ diagrams (Figure 8). They can be fitted to a ion filtration model of Agrinier et al. (2019) using a boundary condition at the sediment-seawater interface to open the top of the sedimentary piles to exchange with seawater ($\delta^{37}Cl$ = 0 ‰ and $[Cl^-]$ = 558 mM). This leads to dilute the $^{37}Cl$-enriched pore fluids that form in the upper part of the pile in contact with seawater.

The partition coefficient of chlorides ($K_{Cl}$) between the expelled fluid and the residual fluid determines the enrichment or the depletion in chlorides with respect to the seawater value ($K_{Cl}$ = $[Cl^-]_{expelled\ fluid}/[Cl^-]_{residual\ fluid}$). Modeled $K_{Cl}$ are always very close to unity at the level of a few percent, reflecting the overall small deviation from the seawater chlorinity within sedimentary piles. Sedimentary piles 997 and C0011 have $K_{Cl}$ of 1.15 and 1.02 respectively and Sedimentary piles 757, 758 and C0012 have $K_{Cl}$ of 0.94, 0.94 and 0.985 respectively. Overall, our model suggest that ion filtration would not partionate a lot chlorides across clay membranes. Sedimentary pile 1150 yields $K_{Cl}$ value at 1.60, significantly above unity because [$Cl^-$] decreases to 307 mM. However, the cause of this decrease in [$Cl^-$] may be the addition of fresh water from the dehydration of hydrated minerals, destabilization of gas hydrates or fresh water advected from the deep levels (Deyhle et al., 2003; Mora, 2005) that could mask the effect of ion filtration on [Cl-] but would have no or very little impact on the $\delta^{37}Cl$.

Chlorine isotope fractionation factors ($K^{37}/K^{35}$) are systematically above 1, ranging between 1.0005 and 1.008, indicating that the expelled chlorides must be enriched in $^{37}Cl$ in comparison to the residual fluid. These chlorine isotope fractionation factors ($K^{37}/K^{35}$) values appear weakly dependent on the $K_{Cl}$ values as long as [$Cl^-$] is within the 400 – 700 mM interval which is generally the case except for the lower part of Sedimentary pile 1150.

Sedimentary piles 1150 fluids fit the model curve with small chlorine isotope fractionation factors between 1.00075 and 1.0005. Such small factors were expected since the $^{37}Cl$-depletion of chlorides is only -1.1 ‰ from the seawater' $\delta^{37}Cl$ value. Although clays are abundant in this sedimentary pile, chlorite/kaolinite is more abundant than smectite.

Sedimentary piles 757 & 758 pore fluids fit the model curve with chlorine isotope fractionation factors of between 1.001 and 1.002. There rather small fractionation factors can be explained by the near absence of clay at the top of these two sedimentary piles, dominated by calcareous ooze (carbonate contents > 70 %). In Sedimentary pile 757, clays, chlorite/smectite, are significantly abundant (i.e. > 50 percent) only below 220 mbsf, in the waterlain ashes and tuffs. Similarly in Sedimentary pile 758, clay, chlorite/smectite, is the dominant component only below 300 mbsf (Peirce et al. 1989c). This suggests that chlorine isotopes were fractionated mostly in the lower units and that resulting $^{37}Cl$-depleted fluids were transported upwards and partially mixed with seawater-like fluid into the upper carbonate ooze. The carbonate ooze tops would not have the capacity to produce $^{37}Cl$-depleted chlorides because they are clay-poor and consequently the chloride electric repulsion by negatively charged clay surfaces is weak. Moreover, the carbonate ooze has reduced capacity to store $^{37}Cl$-depleted chlorides because of their relatively high permeability in comparison to clay-rich sediments.

Sedimentary piles 646 & 997 fit the model curve with chlorine isotope fractionation factors of 1.003. Carbonate contents are low in these piles (≤ 25 %). In Sedimentary pile 646, the abundances of smectites and illites largely dominate that of chlorites at the top of the sedimentary pile and the abundance of smectite steady increases with depth. (Cremer et al., 1989). Sedimentary pile 997 clay abundance is large and constant but the nature of clays has not been determined (Paull et al., 1996). As seen above, these sedimentary piles present unusual geochemical features: [$Ca^{2+}$] and $\delta^{18}O$ are unchanged from seawater values whereas [$Mg^{2+}$] is consumed.

Sedimentary piles C0011 and C0012 fit the model curve with chlorine isotope fractionation factors of 1.004-1.008. These large fractionation factors are obtained for sedimentary piles with large abundance of clays (smectites and mixed-layer clay minerals, Underwood; 2000) and low carbonate contents (<10%).

From this set of « regular compaction» sedimentary piles, there appears to be a close relationship between the abundance of clays in the sedimentary pile and the chlorine isotope fractionation. The higher the clay abundance, the larger the chlorine isotope fractionation. In particular, large chlorine isotope fractionations are obtained when clays dominated by smectites. The ages of the $^{37}$Cl-depletion maxima are all in the 6 to 19 Ma age interval.

The sedimentary piles 645, 647 and 1201 are older; they have complex histories of sedimentation involving lithologic discontinuities and sedimentary hiatuses. They display non-regular porosity profiles (Figure sup 1) that cannot be fitted with a single compaction equation of Athy (1930) over the whole drilled hole. However, in non-perturbed sedimentary intervals , a $\delta^{37}$Cl – $F_{chloride}$ relationships appears (Figures 9, 10 & 11)

Sedimentary pile 645 data are divided in two intervals on the basis of the lithology and porosity profiles (Srivastava et al., 1987d; Bush, 1989; Figure sup 1). In the shallow depth interval, 0 to 200 mbsf, lithology is made of calcareous silty clays deposited by turbidity currents and clay mineralogy is dominated by illite and chlorite. In the bottom depth interval, below 200 mbsf, lithology is made of sand-bearing silty muds with clay mineralogy dominated by smectite (Thiebault et al., 1989). The shallow interval data fit the ion filtration model curves with chlorine isotope fractionation, in the 1.001-1.002 range while those of the bottom interval fit the ion filtration model curves with large chlorine isotope fractionations in the 1.005-1.007 range (Figure 9).

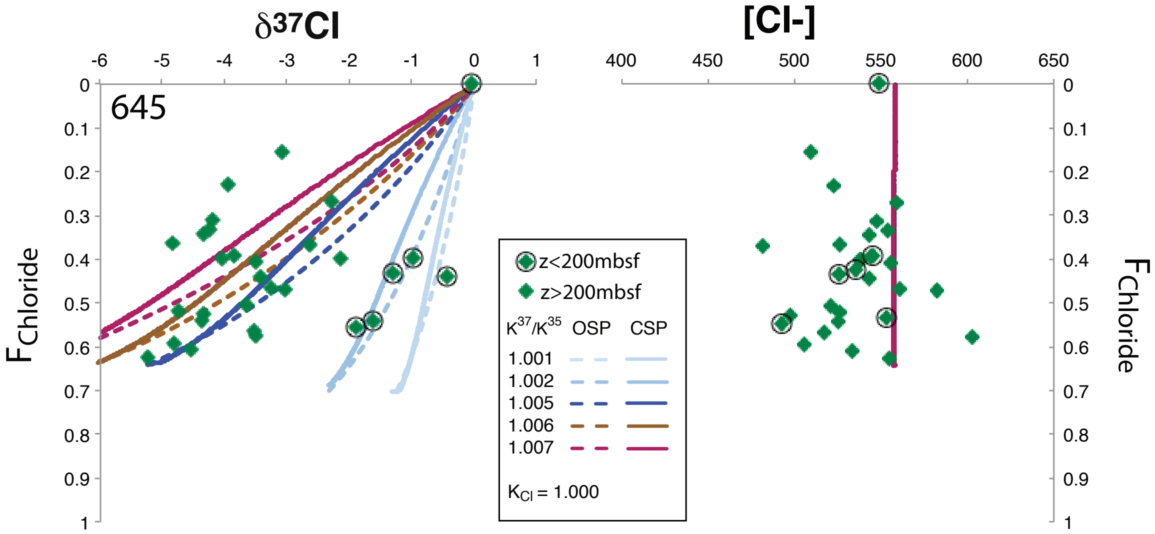


***Figure 9:*** *The $\delta^{37}$Cl – $F_{chloride}$ relationship for Sedimentary pile 645. Above 200 mbsf, clay mineralogy is dominated by illite and chlorite while it is dominated by smectite below 200 mbsf. The $\delta^{37}$Cl – $F_{chloride}$ relationships for the pore fluids sampled above 200 mbsf can be fitted with compaction-induced ion filtration model curves with chlorine isotope fractionation between 1.001 and 1.002, while that for the pore fluids below 200 mbsf requires chlorine isotope fractionation larger than 1.005.*

Sedimentary pile 647 is also divided in two intervals. The shallow depth interval (z < 140 mbsf) and the bottom depth interval (z > 140 mbsf) are separated by a 10 Ma sedimentation hiatus in the Miocene times. This limit corresponds to a change in the mode of sedimentation from ice rafting and bottom currents above to hemipelagic sedimentation below (Bush, 1989; Srivastava et al., 1987d). The shallow depth interval data plot close the ion filtration model at 1.001 whereas those of bottom depth interval fit the ion filtration model with chlorine isotope fractionation of 1.003 to 1.004 (Figure 10).

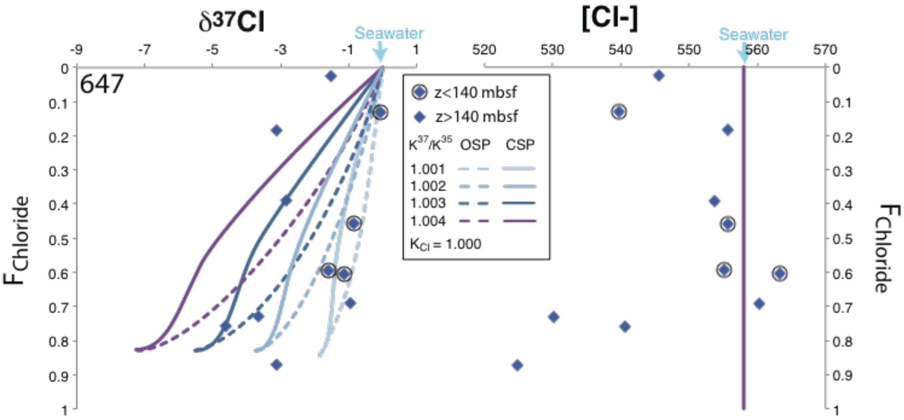


*Figure 10: The $\delta^{37}Cl$ – $F_{chloride}$ relationship for Sedimentary pile 647. Above 140 mbsf, where a major hiatus occurs, clay mineralogy is dominated by Illite and chlorite while it is dominated by smectite under 140 mbsf.*

Mineralogy of the bottom depth interval is largely dominated by smectites whose abundance is constant, at about 50 % (Nielsen et al., 1989). Clays of unknown mineralogy dominate the shallow depth interval.

Site 1201 is the only sedimentary pile where pore fluid chloride content increases markedly with depth (Figure 3). Only data from the bottom depth interval (i.e. below the two sedimentary hiatuses Miocene and Oligocene times, z > 200 mbsf) are available. They can be fitted with the ion filtration model curves with chlorine isotope fractionation between 1.004 and 1.005 and $K_{Cl}$ as small as 0.82 (Figure 11). In the upper part, z < 200 mbsf, the lithology is made of interbedded sandstone and bioturbated silty claystone with breccia deposited by turbidity currents, mineralogy is dominated by expandable and poorly crystallized clay minerals. Below 200 mbsf, a marked change in clay mineralogy is evident with the appearance of well-crystallized smectite downhole (Salisbury et al., 2002).

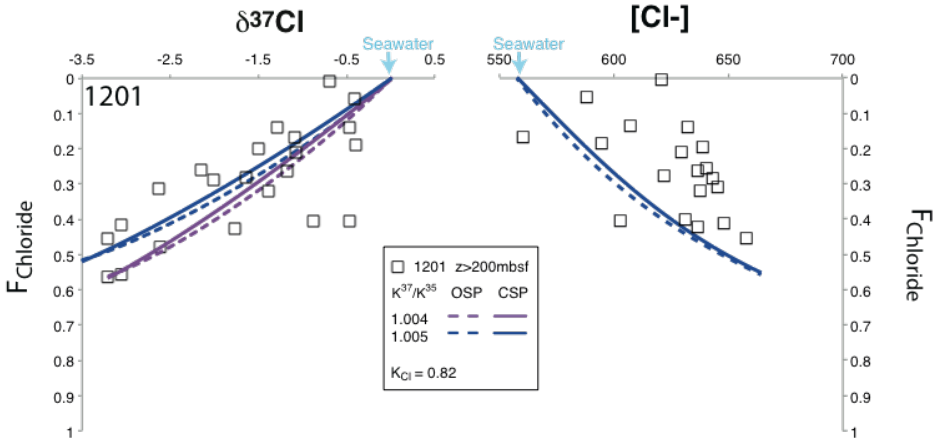


*Figure 11 : The $\delta^{37}Cl$ – $F_{chloride}$ relationship for Sedimentary pile 1201. Only chlorides from the bottom interval (i.e. below the two sedimentary Miocene and Oligocene hiatuses, z >*

*200 mbsf) can be fitted with the compaction-induced ion filtration model curves with chlorine isotope fractionation between 1.004 and 1.005 and $K_{Cl}$ as small as 0.82.*

In the smectite-rich intervals of these three « perturbed » sedimentary piles suggested $\delta^{37}Cl$ – $F_{chloride}$ relationships fit the ion filtration model with large chlorine isotope fractionations (in the 1.003-1.005 range).

Sedimentary piles 1026, 1028 and 1030 are younger than 1.5 Ma and display porosities that undergo only small reduction with burial. As a consequence, compaction equation parameters cannot be easily estimated. However approximate relationships between $\delta^{37}Cl$ and $F_{chloride}$ can be suggested (Figure 12). For these three young sedimentary piles, small chlorine isotope fractionations, in the 1.003-1.001 interval are inferred. In these piles, clay mineralogy is dominated by illite and chlorite+kaolinite while smectites and carbonates are minor components (Underwood and Hoke, 2000).

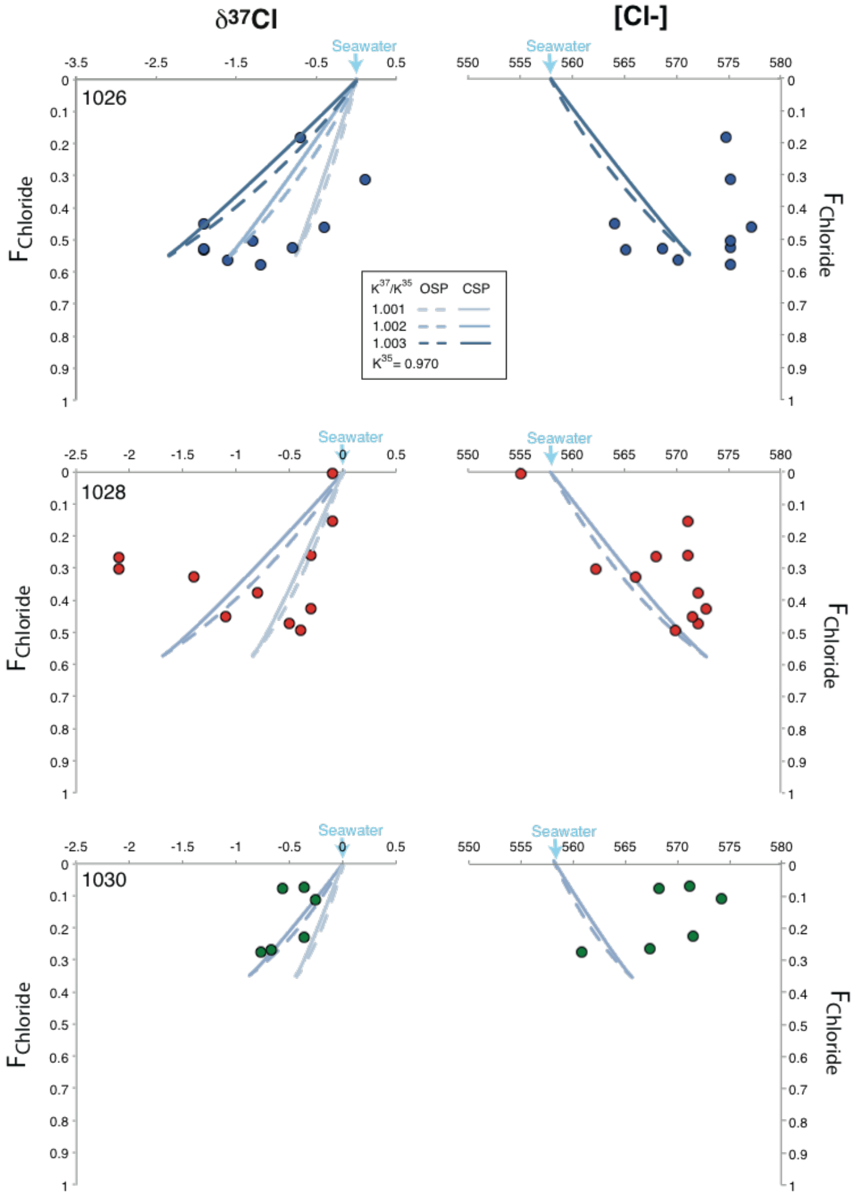


***Figure 12** : The $\delta^{37}Cl$ – $F_{chloride}$ relationships for Sedimentary piles 1026, 1028 and 1030. The compaction-induced ion filtration model curves with small chlorine isotope fractionation, lower than 1.003, can fit the chlorine data.*

The compaction-induced ion filtration modeling of this set of 13 clay-rich sedimentary piles shows that large chlorine isotope fractionations are obtained when clays are dominated by smectites. For clays dominated by illite, chlorite and kaolinite, small chlorine isotope fractionations are obtained, whereas null or very small chlorine isotope fractionations are obtained for carbonate-rich sediments. In all cases but one, the value of the $K_{Cl}$, the partition coefficient of chlorides between the expelled fluid and the residual fluid obtained is very close to unity, suggesting that ion filtration of chlorides through clay membrane would only have a small impact on [$Cl^-$]. This is surprising if the negative charges of the clay membrane surfaces repel chloride ions and thus would slow the passage of chlorides through the clay membranes as envisaged in the Phillips and Bentley ion filtration theory. In this case $K_{Cl}$ values would be well below 1, thus producing an increase in chlorinity as a function of depth. Such profiles of chlorinity are not observed and this suggests the effects of ion filtration on chlorinity are small.

### *IV.2)* Oxygen isotope compositions of pore fluids and the $\delta^{18}O$-$\delta^{37}Cl$ relationships

The oxygen isotope compositions of the pore fluids left in these clay-rich sediments are systematically depleted in $^{18}O$ in comparison to the seawater originally contained in pore fluids. This is usually interpreted as the result of water-rock exchanges during which $^{18}O$ is sequestrated in $^{18}O$-enriched minerals, mainly clays, at the expense of the pore fluids (Lawrence et al., 1975; Lawrence and Gieskes, 1981 and many later works). However these works report that in the sediments , the water-rock exchange process is not sufficient to produce large $^{18}O$-depletions i.e. to produce $\delta^{18}O$ of pore fluids ≤ -3 ‰). For the sedimentary piles studied here, the closed system model of Lawrence (Figure 13) shows that in situ production of authigenic clay at 25 °C from detrital clay or basaltic ash is capable of lowering the $\delta^{18}O$ of pore fluids of 6 ‰ but it requires the oxygen of all detrital clays to be requilibrated with that of the pore fluids. This is because the molar fraction of oxygen in the pore fluids is large (> 0.25) for porosity larger than 0.35 and because part of sediment is made of non-exchangeable oxygen atoms (in detrital quartz and feldspaths, at the million year scale and temperatures below 100°C). The production of $^{18}O$-depleted pore fluids with $\delta^{18}O$ below -4 ‰ through oxygen exchange between detrital clays or ash and pore fluids is not possible at higher temperatures (≥ 50°C) because the oxygen isotope fractionation between clay and water decreases too rapidly with the elevation of temperature. Another possibility to decrease the $\delta^{18}O$ of pore fluids is the formation of clay from volcanic ashes, but such material is generally rare or localized at some levels in the sediment (< 10 % in mass, that is oxygen molar fractions lower than 0.26) and cannot explain $^{18}O$ depletions as low as -6 ‰.

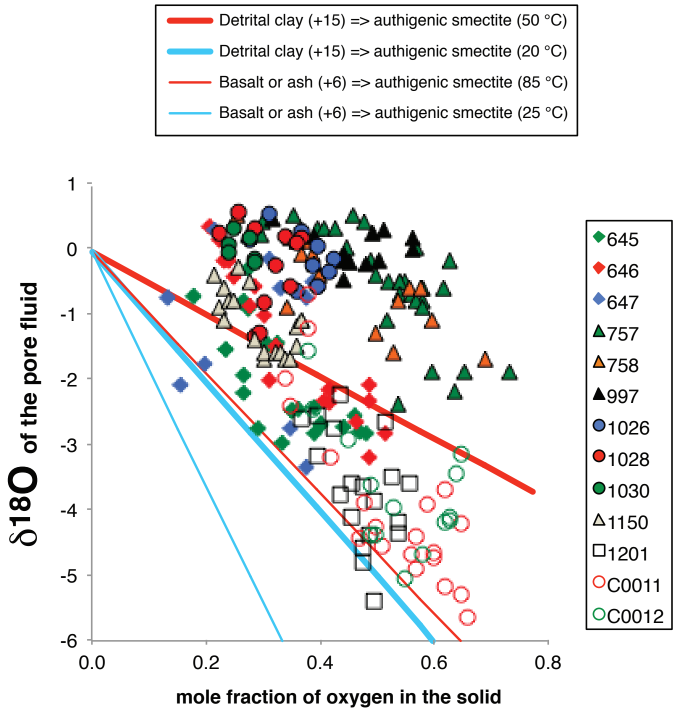


***Figure 13 :*** *The $\delta^{18}O$ of the pore fluid model of Lawrence et al. (1975) allows to compute the expected $\delta^{18}O$ of the pore fluid after alteration of detrital clay or basaltic ash to authigenic smectite under isotopic equilibrium conditions in a closed system. The $\delta^{18}O$ of the pore fluid is plotted as a function of the mole fraction of oxygen in the clay or basalt/basaltic ash. Thick lines describe the reaction of detrital clay to authigenic smectite at 50°C and 20°C. Thin lines describe the reaction of basalt/basaltic ash to authigenic smectite at 85°C and 25°C. The initial $\delta^{18}O$ values of the detrital clay, basalt or ash are +15‰ and +6‰ respectively. The equilibrium fractionation factors between authigenic clay and water are from Sheppard and Gilg (1996).*

In consequence, the in situ alteration of the sediment is not capable of explaining the large $^{18}O$ depletion found in many of these pore fluids. By compiling pore fluid data from a large number of sites, Lawrence and coworkers noticed these oxygen isotope balance problems and a similar balance discrepancy for $Ca^{2+}$. These led them to suggest complementary $^{18}O$-depleted and $Ca^{2+}$-enriched flux from the underlying basalts of layer 2 into the overlying sediments (Lawrence et al., 1975; Lawrence and Gieskes, 1981). Meanwhile, in the basalts of layer 2, $^{18}O$-depleted pore fluids as low as $\delta^{18}O$ = -6 ‰ have not been found. These problems show that the water-rock exchange is not fully satisfactory to explain the changes in $Ca^{2+}$ and in $^{18}O$ in pore fluids of clay-rich oceanic sediments .

Alternatively, a solution to these oxygen balance problems might be an oxygen isotope fractionation produced during the filtration of the pore fluids by clay in the sediment. $^{18}O$-depleted pore fluid would form if $H_2{}^{18}O$ is expelled out by filtration through clay membranes more readily than $H_2{}^{16}O$. Haydon and Graf (1986) measured such an oxygen isotope fractionation, however small ($\delta^{18}O_{upstream}$ - $\delta^{18}O_{downstream}$ = 0.05 ‰ at 180°C to 0.15 ‰ at 140°C) in centimeter thick smectite membranes through which brines where forced for up to 6 months. Integrating that small isotope fractionation over the scales of sedimentary piles, i.e. hundreds of meters, and hundreds of thousands of years, may lead to large isotope effects. Meanwhile, Demir (1988) later observed contradicting oxygen isotope fractionation during similar experiments. The $^{18}O$-depletion in the pore fluids is also in opposition to the suggestion by Philipps and Bentley (1987) in which the oxygen isotope fractionation would be controlled by the larger activity of heavy water molecules ($HD^{16}O$ and $H_2{}^{18}O$) in the membrane in comparison to that of light water molecules ($H_2{}^{16}O$). Another mechanism must be found to explain the $^{18}O$-depletion of pore fluids during ion filtration. So all this gives matters for a debate and shows the fractionation of oxygen isotopes of water during filtration by clay needs more experimental and theoretical attentions.

Overall, in the literature about pore fluids from the oceanic crust, the water-rock exchange with additional $^{18}O$-depleted-$Ca^{2+}$-enriched flux is by far preferred to filtration. Nevertheless, the $^{18}O$-$^{37}Cl$ relationships bring constraints on the processes that produced the $^{18}O$- and $^{37}Cl$-depletions:

The $^{18}O$-$^{37}Cl$ relationships are very robust since they include pore fluids from various oceanic contexts and covering a large interval of ages from 0 to 55 Ma. Perturbations of sediment diagenesis had no impact on them or the changes in $^{18}O$ were highly correlated with that in $^{37}Cl$. The main trend fitting through most of the sedimentary piles (646, 647, 757, 758, 1028, 1030, C0011 & C0012, Figure 6) points towards the same endmember, A1', indicating that the process(es) that produced the $^{18}O$-$^{37}Cl$ relationships is(are) widely occurring. The common feature of these sediments is the presence of clays whose mineralogy (smectite, illite-chlorite) and abundance do not appear to influence the slope of the $^{18}O$-$^{37}Cl$ relationship, but they influence the amplitude of the $^{18}O$-$^{37}Cl$- coupled depletions. Endmember A1', which is the most extreme in terms of isotopes ($\delta^{37}Cl$ = -8.52 ‰; $\delta^{18}O$ = -5.66 ‰) and chemistry ($Ca^{2+}$ = 47 mM; $Mg^{2+}$ = 1.7 mM), would be the fluid most affected by the process that reacts seawater in the clay-rich sediments. Particular processes, such as local injections of exogenous fluids depleted in $^{18}O$ and in $^{37}Cl$ like endmember A1', into the sedimentary piles, can hardly explain the worldwide generalization of the main trend. Indeed, local injected external fluids at the favour of highly permeable sediment layers can occur (Agrinier et al., 2019).

Most of the slopes of the $^{18}O$-$^{37}Cl$ relationships are close to unity showing that the depletions in $^{18}O$ and in $^{37}Cl$ are of similar magnitudes (Figures 6 and sup. 2). Adapting the compaction-induced ion filtration model of Agrinier et al. (2019) to oxygen isotopes of water allows computing the oxygen isotope fractionations between the expelled fluid and the residual fluid for each sedimentary pile. They are maxima values since in this modeling we make the assumption that the contribution of water-rock exchanges is null. The modeled fractionation factors are in the 1.001-1.005 interval and correlate positively with the chlorine isotope fractionation factors (Figure 14). This correlation is expected since the depletions in $^{37}Cl$ and in $^{18}O$ are strongly correlated. The slope of the relationship between O and Cl isotope fractionations is about 0.6 suggesting that the oxygen isotope fractionations are slightly smaller than those of chlorine isotopes. This modeling shows that even small oxygen isotope fractionations can explain the 5 ‰ $^{18}O$-depletion of the pore fluids by a process such as compaction-induced ion filtration. As said above, these oxygen isotope fractionations, above unity, are consistent in direction with the results of Haydon and Graf (1986), not consistent with those of Demir (1988) and contradictory with the mechanism suggested by Phillipps and Bentley (1987).

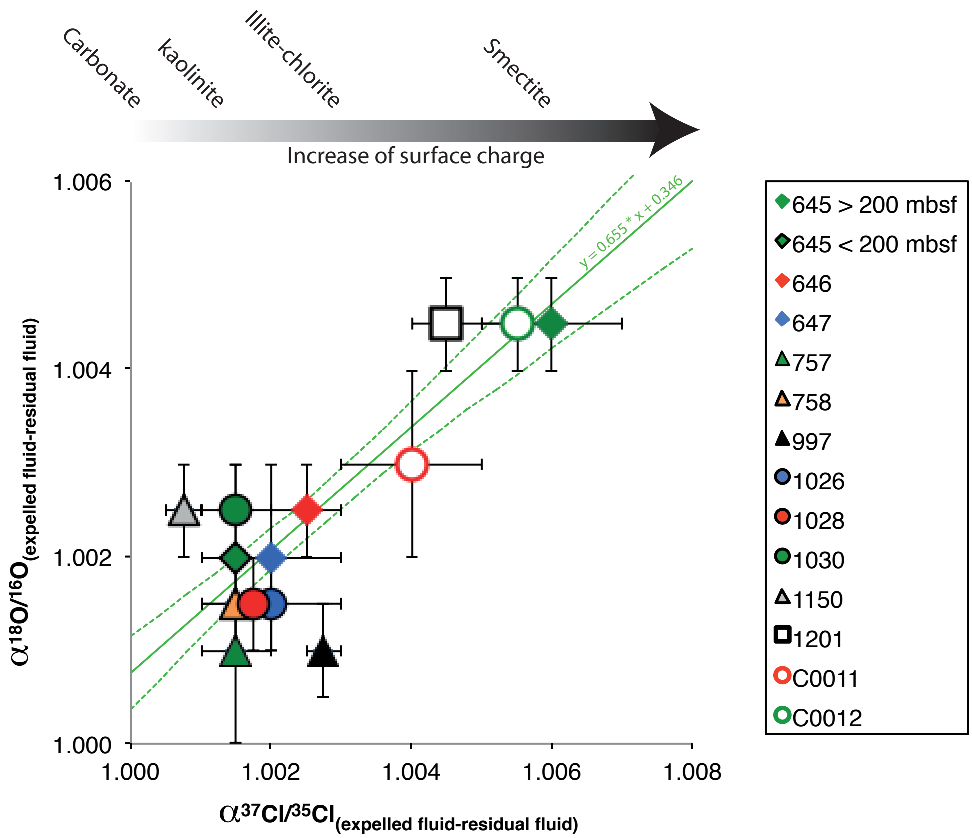


***Figure 14:*** *Comparison of oxygen and chlorine isotope fractionation factors between the expelled fluid and the residual pore fluid required to explain the $^{18}O$ and $^{37}Cl$-depletions in the studied pore fluids. These fractionation factors were calculated by adjusting the compaction-induced ion filtration model of Agrinier et al. (2019) to the $\delta^{18}O$ and $\delta^{37}Cl$ depth profiles. A positive correlation exists between oxygen and chlorine isotope fractionation factors at a confidence level better than 99.9 %. The slope is 0.66 ± 0.14 and intercept is 0.35 ± 0.14. Such a relationship is expected from the $^{18}O$-$^{37}Cl$ relationships observed in Figure 6. The arrow at the top suggests a relationship between the isotope fractionations and the dominant mineralogy (carbonate vs clays) of the sediments, probably through the surface charge of the minerals (as measured by the cationic exchange capacity).*

Considering the relationships between $Ca^{2+}$ and $\delta^{18}O$ (Figure 5) and that between $\delta^{18}O$ and $\delta^{37}Cl$ (Figure 6), it seems that ion filtration process might play a role in the enrichment in $Ca^{2+}$ of these pore fluids. The ion filtration model demands $K_{Ca}$ (= $[Ca^{2+}]_{\text{expelled fluid}}/[Ca^{2+}]_{\text{residual fluid}}$) below unity to explain the increase of $Ca^{2+}$. Enrichment in $Ca^{2+}$ up to 30 mM are obtained only for decreasing $K_{Ca}$ to very small value (< 0.1) thus showing that this modeling of ion filtration is unable to reproduce the highest enrichments in $Ca^{2+}$ (up to 239 mM in 1201 and 151 mM in 757). It is not reasonable to explain all of the $Ca^{2+}$ increase by ion filtration, a significant portion of the $Ca^{2+}$ increase must include contributions from the water-rock exchange that releases $Ca^{2+}$ from the minerals to the pore fluids.

In short, we are facing a problem: a model of compaction-induced ion filtration can explain the coupled depletions in $^{18}O$ and $^{37}Cl$. This model requires chlorine and oxygen isotope fractionation factors controlled by the nature of clays. Smectites would produce large isotope fractionations, illites-chlorites-kaolinites would produce intermediate or small isotope fractionations, and carbonates would produce null isotope fractionations. The idea of compaction-induced ion filtration invokes only one process but would call for a revision of accepted interpretations of the $^{18}O$ changes in pore fluids. The alternative explanation, based on accepted knowledge on pore fluid geochemistry, calls for water-rock exchanges to explain the $^{18}O$, $Mg^{2+}$, $Ca^{2+}$ changes and a fluid-specific process, such as ion filtration, to explain the $^{37}Cl$-depletions. In this case, our results suggest that both processes, the water-rock exchanges and the fluid-specific process are strongly coupled in clay-rich sedimentary piles.

## V) Broader implications

Beyond the clay-rich sediment pore fluids in the oceanic crust, our study clearly shows that chloride concentrations, may no longer be considered as a conservative tracer as proven by the chlorine isotope compositions. Regardless of the mechanism that created the $^{37}Cl$-depleted chlorides in clay-rich oceanic sediment, the low temperature minerals do not have the capacity to store the missing $^{37}Cl$-enriched chlorides. Hence, as said in §IV.1, the law of conservation of isotopes leads to infer that missing $^{37}Cl$-enriched chlorides were expelled out of the sediments into the seawater. This inferred flux of chlorides, out of the sediment into the seawater, is very likely associated to fluxes of other components of pore fluids such as water and dissolved ions (at least to compensate for negative charges). In consequence, part of the dynamic of these geochemical tracers, interpreted to result from water-rock exchanges or to the changes of seawater composition ($^{18}O/^{16}O$, [$Cl^-$]), might be due to an in situ fluid-specific process such as ion filtration.

This study shows that clay-rich oceanic sediments are places where water-rock interactions, via ion filtration and/or water-rock exchanges, produce large and coupled fractionations of oxygen and chlorine stable isotopes in fluids. It is then likely that similar isotopic fractionations would develop in other contexts where clays and fluids interact such as soils, deep aquifers, etc. But their recognition might be difficult because it could be masked by the variability of the initial $\delta^{18}O$ and $\delta^{37}Cl$ of the fluids. That does not happen for the oceanic clay-rich sediments in which the initial pore fluids are always seawater with relatively constant $\delta^{18}O$ and $\delta^{37}Cl$ values.

As chlorides in porefluids of oceanic clay-rich sediments are $^{37}Cl$-depleted, subduction metamorphism formed minerals, such as hydrous phyllosilicates, amphiboles and lizardite, that incorporate chlorides from pore fluids must also be $^{37}Cl$-depleted since the equilibrium isotopic fractionation between silicates and fluid is small, not exceeding 2‰ at 400 °C (Balan et al., 2019). As a consequence, the flux of chlorides into the subduction zones must be depleted in $^{37}Cl$ as measured in subducted rocks by Barnes et al. (2006, 2019); Bonifacie et al. (2008); Selverstone and Sharp (2015).

## VI) Conclusions

We show above that the chlorides of the pore fluids in oceanic clay-rich sediments are systematically depleted in $^{37}Cl$ in comparison to their original source: the seawater. This depletion is large for smectites-dominated sediments, intermediate for Illite/chlorites-dominated sediments and small or null for carbonate-dominated sediments. Thus showing that mineralogy of the clays might control the chlorine isotope fractionations in fluids. The $^{37}Cl$-depletion is observed in a large variety of tectonic contexts. This generality implies that its cause must be a process that occurs in any sediments and suggests that particular processes, such as the invasion by external fluids; diffusion of chlorides cannot be the cause of the depletion of $^{37}$Cl in chlorides. Ion filtration induced by compaction of clay-rich sediment is an in situ process that has the capacity to produce the observed $^{37}$Cl depletions.

These $^{37}$Cl-depletions are systematically strongly correlated to $^{18}$O-depletions in water of pore fluids. A common process that would fractionate both oxygen and chlorine isotopes in fluids, such as ion filtration, might be the cause of that but more experiments are needed since existing experimental filtrations of fluids by smectite membranes were shown to display opposite, and therefore inconsistent, oxygen isotope fractionations in the permeates. On the other hand, two strongly coupled processes, one that would fractionate oxygen isotopes, such as water-rock exchanges and the other, chlorine isotopes; such as ion filtration might as well be the causes.

**Acknowledgments** The International Ocean Discovery Program (IODP), the Bremen Core Repository (University of Bremen, Germany) and Kochi Core Center (Kochi University, Japan) for sampling, storing and making available the pore fluids analyzed in this work. We thank C. Monnin for having provided samples from ODP Leg 168. The TelluS Program of CNRS/INSU and the Comité IODP-France supported the CloPorT project. We are grateful to Miriam Kastner who kindly gave advices and comments on a previous version of this work. The authors thank Laurence Coogan and Antony Gargano for their comments and suggestions. We thank Nicholas Tosca for editing this work and his help in improving our presentation. This is Institut de Physique du Globe de Paris contribution 4200.

## References

Agrinier P., Destrigneville C., Giunta T., Bonfacie M., Bardoux G., Andre J. and Lucazeau F. (2019) Strong impact of ion filtration on the isotopic composition of chlorine in young clay-rich oceanic sediment pore fluids. Geochim. Cosmochim. Acta **245**, 525–541.

Athy, L.F. (1930) Density, porosity, and compaction of sedimentary rocks. AAPG Bull. **14**,1-24.

Barnes, J.D., Selverstone, J., Sharp, Z.D. (2006) Chlorine isotope chemistry of serpentinites from Elba, Italy, as an indicator of fluid source and subsequent tectonic history. Geochem. Geophys. Geosyst. **7-8**, 1-14. doi:10.1029/2006GC001296

Barnes, J.D. and Cisneros M. (2012) Mineralogical control on the chlorine isotope composition of altered oceanic crust. Chemical Geology **326-327**, 51-60.

Barnes, J.D., Penniston-Dorland S.C., Bebout G.E., Hoover W., Beaudoin G.M., Agard P. (2019), Chlorine and lithium behavior in metasedimentary rocks during prograde metamorphism: A comparative study of exhumed subduction complexes (Catalina Schist and Schistes Lustrés). Lithos **336–337**, 40–53.

Berner R.A. (1980) Early Diagenesis, A Theoretical Approach. Princeton Series in Geochemistry. Princeton University Press.

Bernachot I., Garcia B., Ader M., Peysson Y., Rosenberg E., Bardoux G. and Agrinier P. (2017) Solute transport in porous media during drying: The chlorine isotopes point of view. Chem. Geol. **466**, 102–115.

Bonifacie M. (2005) Le cycle du Chlore terrestre : les échanges manteau-océan. Ph. D. thesis IPGP-Universite´ Paris VII- Denis Diderot, 300pp.

Bonifacie M., Monnin C., Jendrzejewski N., Agrinier P. and Javoy M. (2007) Chlorine stable isotopic composition of basement fluids of the eastern flank of the Juan de Fuca Ridge (ODP Leg168). Earth Planet. Sci. Lett. **260**, 10–22.

Bonifacie M., Busigny V., Mevel C., Philippot P., Agrinier P., Jendrzejewski N., Scambelluri M., Javoy M. (2008) Chlorine isotopic composition in seafloor serpentinites and high-pressure metaperidotites. Insights into oceanic serpentinization and subduction processes. Geochim. Cosmochim. Acta, **72**, 126-139.

Bonifacie M. (2017) Chlorine Isotopes In Encyclopedia of Geochemistry. Editor Bill White, Publish. Springer

Bush W.H. (1989) Patterns of sediment compaction at ocean drilling program Sites 645, 646, and 647, Baffin Bay and Labrador Sea. In Srivastava, S. P., Arthur, M., Clement, B., et al., 1989. Proc. ODP, Sci. Results College Station, TX (Ocean Drilling Program) **105**, 781-790.

Campbell D.J. (1985) Fractionation of stable chlorine isotopes during transport through semipermeable membranes. Ms Thesis The University of Arizona. 103pp. http://hdl.handle.net/10150/191280.

Cramer B.S., Miller K.G., Barrett P.J. and Wright J.D. (2011) Late Cretaceous–Neogene trends in deep ocean temperature and continental ice volume: Reconciling records of benthic foraminiferal geochemistry ($\delta^{18}$O and Mg/Ca) with sea level history. Jr Geophys. Res. **116**, C12023, doi:10.1029/2011JC007255,

Cremer M., Maillet N. and Latouche C. (1989) Analysis of sedimentary facies and clay mineralogy of the neogene-quaternary sediments in ODP Site 646, Labrador Sea. In Srivastava, S. P., Arthur, M., Clement, B., et al., 1989. Proc. ODP, Sci. Results College Station, TX (Ocean Drilling Program) **105**, 71-81.

Coleman M.L., Eggenkamp H.G.M. and Aranyossy, J.-F. (2001) Chlorine stable isotope characterisation of solute transport in mudrocks. ANDRA: Actes des journées scientifiques 1999. **Chapter 10**, 155-175, EDP Sciences, France.

Davis, E.E., Fisher, A.T., Firth, J.V., et al. (1997a) Introduction and Summary : Hydrothermal circulation in the oceanic crust and its consequences on the eastern flank of the Juan de Fuca ridge. Proc. ODP, Init. Repts, College Station, TX (Ocean Drilling Program). **168**, 7-21

Davis, E.E., Fisher, A.T., Firth, J.V., et al. (1997b) Rough basement transect (Sites 1026 and 1027). Proc. ODP, Init. Repts College Station, TX (Ocean Drilling Program). **168**, 101-160.

Davis, E.E., Fisher, A.T., Firth, J.V., et al. (1997c) Buried basement transect (Sites 1028, 1029, 1030, 1031, and 1032). Proc. ODP, Init. Repts College Station, TX (Ocean Drilling Program). **168,** 161-212.

Demir I. (1988) Studies of smectite membrane behavior: Electrokinetic, osmotic, and isotopic fractionation processes at elevated pressures. Geochim. Cosmochim. Acta **52**, 727-737.

Destrigneville C., Agrinier P., Henry P. and Torres M. E. (2016), Data report: d18O in pore fluids from NanTroSEIZE Expeditions 322 and 333. In Proceedings of the Integrated Ocean Drilling Program, 322 (eds. S. Saito, M. B. Underwood and Y. Kubo) and the Expedition 322 Scientists. Integrated Ocean Drilling Program Management International, Inc., Tokyo. **322**, 1-6. doi:10.2204/iodp.proc.322.212.2016.

Deyhle A., Kopf A., Frape S. and Hesse R. (2003) Evidence for fluid flow in the Japan Trench forearc using isotope geochemistry (Cl, Sr, B): Results from ODP Site 1150. The Island Arc **13**, 258–270.

Deyhle A., Kopf A. and Pawlig S. (2004) Cross-section through the frontal Japan Trench subduction zone: Geochemical evidence for fluid flow and fluid–rock interaction from DSDP and ODP pore waters and sediments. The Island Arc **13**, 271–288.

Eastoe C.J., Long A., Land L.S. and Kyle J.R. (2001) Stable chlorine isotopes in halite and brine from the Gulf Coast Basin: brine genesis and evolution. Chemical Geology **176**, 343–360.

Eggenkamp H.G.M. (1994) $\delta^{37}$Cl: The Geochemistry of Chlorine Isotopes. Ph.D. Thesis. Utrecht University, Utrecht. DOI 10.1007/978-3-642-28506-6.

Eggenkamp H.G.M. and Coleman M. L. (2009) The effect of aqueous diffusion on the fractionation of chlorine and bromine stable isotopes. Geochim. Cosmochim. Acta **73**, 3539–3548.

Eggenkamp H.G.M. (2010) The Geochemistry of Stable Chlorine and Bromine Isotopes. Advances in Isotope Geochemistry, Springer 172 pp.

Eggenkamp H.G.M., Bonifacie M., Ader M. and Agrinier P. (2016) Experimental determination of stable chlorine and bromine isotope fractionation during precipitation of salt from a saturated solution. Chemical Geology **433**, 46-56.

Eggenkamp H.G.M., Louvat P., Griffioen J. and Agrinier P. (2019) Chlorine and bromine isotope evolution within a fully developed Upper Permian natural salt sequence. Geochim. Cosmochim. Acta **245**, 316–326.

Epstein, S., and Mayeda, T. (1953) Variations in $^{18}$O content of waters from natural sources. Geochim. Cosmochim. Acta, **27**, 213-224.

Gieskes, J. M. (1974) Interstitial water studies, Leg 25. In Simpson, E.S.W., Schlich, R., et al., Init. Repts. DSDP, Washington (U.S. Govt. Printing Office) **25**, 361-394.

Gieskes, J. M., and Lawrence J.R. (1976) Interstitial water studies, Leg 35. Initial Rep. DSDP. **35**, 407-424.

Gieskes J. M. and Lawrence J. R. (1981) Alteration of volcanic matter in deep sea sediments: evidence from the chemical composition of interstitial waters from deep sea drilling cores. Geochim. Cosmochim. Acta **45**, 1687–1703.

Giunta T. (2015) Isotopes stables du chlore et du brome en milieu poreux. Ph. D. thesis IPGP-Universite´ Paris VII- Denis Diderot, 300pp.

Giunta T., Devauchelle O., Ader M., Locke R., Louvat P., Bonifacie M., Métivier F. and Agrinier P. (2017a) The gravitas of gravitational isotope fractionation revealed in an isolated aquifer. Geochemical Perspectives Letters **4**, 53-58.

Giunta, T., Labidi, J. and Eggenkamp, H. G. (2017b) Chlorine isotope fractionation between chloride ($Cl^-$) and dichlorine ($Cl_2$). Geochim. Cosmochim. Acta **213**, 375-382.

Gue, A., Grasby, S.E. and Mayer B. (2018) Influence of saline groundwater discharge on river water chemistry in the Athabasca oil sands region – A chloride stable isotope and mass balance approach. Applied Geochemistry **89**, 75-85.

Godon A., Jendrzejewski N., Castrec-Rouelle M., Dia A., Pineau F., Boulègue J. and Javoy M. (2004a) Origin and evolution of fluids from mud volcanoes in the Barbados accretionary complex. Geochim. Cosmochim. Acta **68**, 2153–2165.

Godon A., Jendrzejewski N., Eggenkamp H. G. M., Banks D. A., Ader M., Coleman M. L. and Pineau F. (2004b) A cross calibration of chlorine isotopic measurements and suitability of seawater as the international reference material. Chemical Geology **207**, 1–12.

Hanshaw, B. B. and T. B. Coplen. (1973) Ultrafiltration by a compacted clay membrane: II. Sodium ion exclusion at various ionic strengths, Geochim. Cosmochim. Acta **37**, 2311–2327.

Haydon P.R and Graf D.L. (1986) Studies of smectite membrane behavior: Temperature dependence, 20-180°C. . Geochim. Cosmochim. Acta **50**, 115–121.

Hendry M., Wassenaar L. and Kotzer T. (2000) Chloride and chlorine isotopes ($^{36}Cl$ and $\delta^{37}Cl$) as tracers of solute migration in a thick, clay-rich aquitard system. Water Resources Research **36**, 285–296.

Henry P., Kanamatsu T. and Moe K.and the Expedition 333 Scientists (2012a) Site C0011, Proc. IODP, 333. Integrated Ocean Drilling Program Management International, Inc., Tokyo, **333**, 1-96. doi:10.2204/iodp.proc.333.104.2012.

Henry P., Kanamatsu T., Moe K.T. and Strasser M.and the IODP Expedition 333 Scientific Party (2012b) IODP Expedition 333: Return to Nankai Trough Subduction Inputs Sites and Coring of Mass Transport Deposits. Scientific Drilling **14**, 4–17. https://doi.org/10.2204/iodp.sd.14.01.2012.

Hesse R., Frape S.K., Egeberg P.K. and Matsumoto R. (2000) Stable isotope studies (Cl, O, and H) of interstitial waters from Site 997, Black ridge gas hydrate field, West Atlantic. Proc. ODP, Sci. Results **164**, 129–137.

Hutchison I. (1985) The effects of sedimentation and compaction on oceanic heat flow. Geophys. J. R. Astr. Soc. **82**, 439–459.

Kaufmann R.S., Long A. and Campbell D.J. (1988) Chlorine isotope distribution in formation waters, Texas and Louisiana: Geologic note. AAPG Bull. **72**, 839–844.

Kendrick M.A. (2018) Halogens in Seawater, Marine Sediments and the Altered Oceanic Lithosphere In The Role of Halogens in Terrestrial and Extraterrestrial Geochemical Processes, D.E. Harlov and L. Aranovich (eds.), , Springer Geochemistry, https://doi.org/10.1007/978-3-319-61667-4._chapter 9, 591-648.

Kharaka, Y. F. and Berry F. A. F. , (1973) Simultaneous flow of water and solutes through geological membranes: I. Experimental investigation, Geochim. Cosmochim. Acta, **37**, 2577–2603.

Kim S.-T. a,nd O'Neil J.R. (1997) Equilibrium and nonequilibrium oxygen isotope effects in synthetic carbonates. Geochim. Cosmochim. Acta **61**, 3461–3475.

Komor S.C. and Mottl M.J. (2006) Data report: pore water chemical and isotopic compositions from the west philippine basin, ocean drilling program Site 1201. In Shinohara, M., Salisbury, M.H., and Richter, C. (Eds.), Proc. ODP, Sci. Results **195**, 1–14

Lavastre V., Jendrzejewski N., Agrinier P., Javoy M. and Evrard M. (2005) Chlorine transfer out of a very low permeability clay sequence (Paris basin, France): $^{35}Cl$ and $^{37}Cl$ evidence. Geochim. Cosmochim. Acta **69**, 4949–4961.

Lawrence J.R., Gieskes J.M. and Broecker W.S. (1975) Oxygen isotope and cation composition of DSDP pore waters and the alteration of layer II basalts. Earth Planet. Sci. Lett. **27**, 1-10.

Lawrence J.R., Drever J.I., Anderson T.F. and Brueckner H.K. (1979) Importance of alteration of volcanic material in the sediments of Deep Sea Drilling Site 323 : chemistry, $^{18}O/^{16}O$ and $^{87}Sr/^{86}Sr$. Geochim. Cosmochim. Acta **43**, 573–588.

Lawrence J.R. and Gieskes J.M. (1981) Constraints on water transport and alteration in the oceanic crust from the isotopic composition of pore water. Jr. Geophys. Res. **86(B9)**, 7924-7934.

Lawrence J.R. (1991) Stable isotopic composition of pore waters and calcite veins. In Weissel, J., Peirce, J., Taylor, E., Alt, J., et al. (1991. Proceedings of the Ocean Drilling Program, Scientific Results **121**, 447-455.

Manheim, F. T, (1966) A hydraulic squeezer for obtaining interstitial water from consolidated and unconsolidated sediments. U.S. Geol. Surv. Prof. Paper 550-C, 256-261.

Mazurek M., Oyama T., Wersin T. and Alt-Epping P. (2015) Pore-water squeezing from indurated shales. Chemical Geology **400**, 106–121.

Mikada, H., Becker, K., Moore, J.C., Klaus, A., et al. (2002a) Site 808. Proceedings of the Ocean Drilling Program, Initial Reports **196**, 1-68. doi:10.2973/odp.proc.ir.196.104.2002

Mikada, H., Becker, K., Moore, J.C., Klaus, A., et al. (2002b) Site 1173. Proceedings of the Ocean Drilling Program, Initial Reports **196**, 1-97. doi:10.2973/odp.proc.ir.196.103.2002

Minster J.-F., Ricard L.-P. and Allègre C.-J. (1978) $^{87}Rb$-$^{87}Sr$ chronology of enstatite meteorites. Earth Planet. Sci. Lett., **44**, 420-440.

Moore, G.F., Taira, A., and Klaus, A., et al. (2001) Proceedings of the Ocean Drilling Program, Initial Reports **190**, 1-146. doi:10.2973/odp.proc.ir.190.105.2001

Mora G. (2005) Isotope-tracking of pore water freshening in the fore-arc basin of the Japan Trench. Marine Geology **219**, 71– 79.

Mottl M.J., Wheat C.G. Monnin C. and Elderfield H. (2000) Data report: trace elements and isotopes in pore water from Sites 1023 through 1032, Eastern flank of the Juan de Fuca ridge. In Fisher, A., Davis, E.E., and

Escutia, C. (Eds.), 2000. Proc. ODP, Sci. Results College Station TX (Ocean Drilling Program) **168**, 105-115.
Musashi, M., Oi, T., Eggenkamp, H.G.M., Yato, Y., Matsuo, M. (2007) Anion-exchange chromatographic study of the chlorine isotope effect accompanying hydration. J. Chromatogr. **A 1140**, 121–125.
Nielsen O.B., Cremer M., Stein R., Thiébault F., and Zimmerman H. (1989) Analysis of sedimentary facies, clay mineralogy, and geochemistry of the paleogene sediments of Site 647, Labrador Sea. In Srivastava, S. P., Arthur, M., Clement, B., et al., 1989. Proc. ODP, Sci. Results College Station, TX (Ocean Drilling Program) **105**, 101-110.
Paull C.K., et al. (1996) Site 997. In Paull, C.K., Matsumoto, R., Wallace, PJ., et al., 1996. Proc. ODP, Init. Repts College Station, TX (Ocean Drilling Program) **105**, 277-334
Paull, Charles K; Matsumoto, Ray; Wallace, Paul J; Shipboard Scientific Party, (2005a) Geochemistry of interstitial water of ODP Hole 164-997A. PANGAEA, https://doi.org/10.1594/PANGAEA.256060.
Paull, Charles K; Matsumoto, Ray; Wallace, Paul J; Shipboard Scientific Party, (2005b) Geochemistry of interstitial water of ODP Hole 164-997B. PANGAEA, https://doi.org/10.1594/PANGAEA.256061
Peirce, J., Weissel, J., et al. (1989a) Leg 121 Background and Objectives: ODP Leg 121, Proc. ODP, Init. Repts., **121**. 1-31.
Peirce, J., Weissel, J., et al. (1989b) Site 757 : ODP Leg 121, Proc. ODP, Init. Repts., **121**. 305-358.
Peirce, J., Weissel, J., et al. (1989c) Site 758 : ODP Leg 121, Proc. ODP, Init. Repts., **121**. 359-453.
Phillips F. M. and Bentley H. W. (1987) Isotopic fractionation during ion filtration: I. theory. Geochim. Cosmochim. Acta **51**, 683–695.
Ransom B., Spivack A. J. and Kastner M. (1995) Stable Cl isotopes in subduction-zone pore waters: Implications for fluid-rock reactions and the cycling of chlorine. Geology **23**, 715–718.
Richter C., Salisbury M., H; Shinohara M., et al. (2005) Shipboard Scientific Party, Geochemistry of interstitial water of ODP Hole 195-1201D. PANGAEA, https://doi.org/10.1594/PANGAEA.256313
Salisbury, M.H., Shinohara, M., Richter, C., et al. (2002) Site 1201. Proceedings of the Ocean Drilling Program, Initial Reports **195**, 1-233. doi:10.2973/odp.proc.ir.195.104.2002
Sacks, I Selwyn; Suyehiro, Kiyoshi; Acton, Gary D; Shipboard Scientific Party (2005a) Geochemistry of interstitial water of ODP Hole 186-1150A. PANGAEA, https://doi.org/10.1594/PANGAEA.256270
Sacks, I Selwyn; Suyehiro, Kiyoshi; Acton, Gary D; Shipboard Scientific Party (2005b) Geochemistry of interstitial water of ODP Hole 186-1150B. PANGAEA, https://doi.org/10.1594/PANGAEA.256271
Saito S. (2010a) Expedition 322 Scientists. Site C0011. In Proc. IODP, 322 (eds. S. Saito, M. B. Underwood and Y. Kubo), and the Expedition 322 Scientists. Integrated Ocean Drilling Program Management International, Inc., Tokyo **322**, 1-159. doi:10.2204/ iodp.proc.322.103.2010.
Saito S. (2010b) Expedition 322 Scientists. Site C0012. In Proc. IODP, 322 (eds. S. Saito, M. B. Underwood and Y. Kubo), and the Expedition 322 Scientists. Integrated Ocean Drilling Program Management International, Inc., Tokyo **322**, 1-121. doi:10.2204/ iodp.proc.322.104.2010.
Selverstone J. and Sharp Z. D. (2013) Chlorine isotope constraints on fluid-rock interactions during subduction and exhumation of the Zermatt-Saas ophiolite. Geochem. Geophys. Geosyst. **14**. 4370-4391. https://doi.org/10.1002/ggge.20269.
Sharp Z.D. and Barnes J.D. (2008) Comment to "Chlorine stable isotopes and halogen concentrations in convergent margins with implications for the Cl isotopes cycle in the ocean" by Wei et al. A review of the Cl isotope composition of serpentinites and the global chlorine cycle. Earth Planet. Sci. Lett. **274**, 531–534
Sheppard S.M.F. and Gilg H. A. (1996) Stable isotope geochemistry of clay minerals. Clay Minerals **31**, 1-24
Spivack A. J., Kastner M. and Ransom B. (2002) Elemental and isotopic chloride geochemistry and fluid flow in the Nankai trough. Geophys. Res. Lett. **29**, 1661–1665.
Srivastava, S. P., Arthur, M., Clement, B., et al. (1987a) Introduction: ODP Leg 105, Proc. Init. Repts. (Part A), ODP **105**, 5-20.
Srivastava, S. P., Arthur, M., Clement, B., et al. (1987b) Site 645: ODP Leg 105, Proc. Init. Repts. (Part A), ODP **105**, 61-418.
Srivastava, S. P., Arthur, M., Clement, B., et al. (1987c) Site 646: ODP Leg 105, Proc. Init. Repts. (Part A), ODP **105**, 419-674.
Srivastava, S. P., Arthur, M., Clement, B., et al. (1987d) Site 647: ODP Leg 105, Proc. Init. Repts. (Part A), ODP **105**, 675-905.
Selverstone J. and Sharp Z. (2015) Chlorine isotope behavior during prograde metamorphism of sedimentary rocks. Earth Planet. Sci. Lett. **417**, 120–131
Thiébault F., Cremer M., Debrabant P., Foulon J., Nielsen O.B. and Zimmerman H. (1989) Analysis of sedimentary facies, clay mineralogy, and geochemistry of the neogene-quaternary sediments in Site 645, Baffin Bay. In Srivastava, S. P., Arthur, M., Clement, B., et al. (1989, Proceedings of the Ocean Drilling Program, Scientific Results **105**, 83-100.
Underwood M.B. and K.D. Hoke. (2000) composition and provenance of turbidite sand and hemipelagic mud in northwestern Cascadia Basin. In Fisher, A., Davis, E.E., and Escutia, C. (Eds.), 2000. Proc. ODP, Sci. Results College Station TX (Ocean Drilling Program) **168**, 51-65.

Underwood M. B., Saito S. and Kubo Y., the Expedition 322 Scientists. (2010) NanTroSEIZE Stage 2: subduction inputs. IODP Prel. Rept. **322**, 1-90. https://doi.org/10.2204/iodp.pr.322.2009.
Wei W., Kastner M. and Spivack A. J. (2008) Chlorine stable isotopes and halogen concentrations in convergent margins with implications for the Cl isotopes cycle in the ocean. Earth Planet. Sci. Lett. **266**, 90–104.
Wei W., Kastner M. and Spivack A. J. (2008b) Reply to comment on: "Chlorine stable isotopes and halogen concentrations in convergent margins with implications for the Cl isotopes cycle in the ocean". Earth Planet. Sci. Lett. **274**, 535.
Zachos J.C., Cederberg T. (1989) Interstitial-Water Chemistry, Leg 105 Sites 645, 646, And 647, Baffin Bay And Labrador Sea. In Srivastava, S. P., Arthur, M., Clement, B., et al., 1989 Proceedings of the Ocean Drilling Program, Scientific Results **105**, 171-183.
Ziegler K. Coleman M.L. and Howarth R.J. (2001) Palaeohydrodynamics of ̄uids in the Brent Group (Oseberg Field, Norwegian North Sea) from chemical and isotopic compositions of formation waters. Applied Geochemistry, 16, 609-632.

## Supplementary Material

### I) Geology of the sedimentary piles

*Sites 645-646-647 of Leg 105* (Srivastava et al., 1987a; Cremer et al., 1989; Thiebault et al., 1989; Nielsen et al., 1989) are located in the North Atlantic Ocean. They document sedimentary piles with decreasing influence of continental influxes and rate of sedimentation. Site 645 is on the continental slope of a narrow failed basin off southern Baffin Island. The sedimentary pile was drilled to 1147 mbsf, into high sedimentation rate, thick sequence of clay-rich terrigenous sediments. Site 646 is located in the Labrador Sea off the southern coast of Greenland, a mature basin that evolved by seafloor spreading. The sedimentary pile was drilled to 760 mbsf, into moderate sedimentation rate thick sequence of clay-rich sediments. Site 647 lies farther in southern Labrador Sea. The sedimentary pile was drilled to 736 mbsf, into relatively low sedimentation rate, thick sequence of clay-rich sediments with a 10 Ma sedimentary hiatus in Miocene times. Site 647 has a terrigenous influx smaller than that of Sites 645 and 646. Conversely the carbonate content increases.

*Sites 757 and 758 of Leg 121* (Peirce, et al., 1989a) lie at the ninetyeast ridge on the rifted fragment of oceanic plateaux in the center of the Indian Ocean. The sedimentary pile 757 was drilled to 421 mbsf, into nannofossil calcareous ooze (0 to 212 mbsf), and altered volcanic ash and tuffs (212 to 369 mbsf) and altered basalts (369 to 421 mbsf). Clays occur below 212 mbsf. The sedimentary pile 758 was drilled to 676.8 mbsf, into Nannofossil ooze with clay (0 to 121.7 mbsf), Nannofossil chalk and clay (121.7 to 367.3 mbsf), volcanic clay (367.3 to 431.2 mbsf). Tuff and basalt occur below 431.2 mbsf. A 10 Ma sedimentary hiatus occurs in the Eocene at 250 mbsf. In these two sedimentary piles, there are marked transitions between the upper parts where carbonates are dominant and the bottom parts where carbonates are almost absent.

*Site 997 of Leg 164* (Paull et al., 1996) is located offshore Carolina, at the foot of the west margin of the Atlantic Ocean. Sedimentary pile 997 was drilled to 750 mbsf, into high sedimentation rate, young clay-rich carbonate-poor sediments which preserved gas hydrates.

*Sites 1026-1028-1030 of Leg 168* (Davis et al., 1997) are along an east-west transect that drilled the Juan de Fuca Ridge east flank young and thin sedimentary piles with distance to ridge decreasing from 100 km (1026) to 40 km (1028 & 1030), East of Pacific Ocean. The sedimentary pile of Site 1026 was drilled to 100 mbsf, into sands and silts, hemipelagic clay-rich sediments. The sedimentary pile of Site 1028 was drilled to

134 mbsf, into sands and silts, hemipelagic clay-rich sediments and reached the basaltic basement below 132 mbsf. The sedimentary pile of Site 1030 was drilled to 48 mbsf, into sands and silts, hemipelagic and clay-rich sediments. Carbonates are rare in these sedimentary piles.

*Site 1150 of Leg 186* (Sacks et al., 2000) is located on the volcanic Arc margin of the Japan Trench plate subduction zone in the west of Pacific Ocean. The sedimentary pile was drilled to 1172 mbsf into young soft hemipelagic diatomaceous ooze and diatomaceous clays changing to hard hemipelagic diatomaceous silty claystone and clayey siltstone at the bottom. Carbonates are rare.

*Site 1201 of Leg 195* (Salisbury et al., 2002) is located in the Northern West Philippine Basin, West of Pacific Ocean. The sedimentary pile was drilled to 510 mbsf in a clay-rich turbiditic sediments (with two large sedimentary hiatuses between 15-24 Ma and 25-30 Ma) and from 510 to 600 mbsf into basaltic basement. Carbonates are rare. The studied pore fluids were taken below the hiatuses (depth > 80 mbsf, i.e. in sediments older than 30 Ma).

*Sites C0011-C0012 of Legs 322 and 333* (Saito et al. 2010a,b ; Henry et al., 2012) are located in the Philippine oceanic plate accretionary prism at the front of the Nankai subduction zone, West of Pacific Ocean. The sedimentary piles of Sites C0011 and C0012 were drilled to 1050 and 550 mbsf, respectively, into Smectite-rich hemipelagic claystones and reached the basaltic basement at the bottom. Carbonates are rare.

This set of thirteen sedimentary piles covers a wide range of tectonic contexts and sedimentation styles. At the bottom of all of them, clay-rich sediments are dominant. At the top, clays may be rare (Sedimentary piles 757, 758).

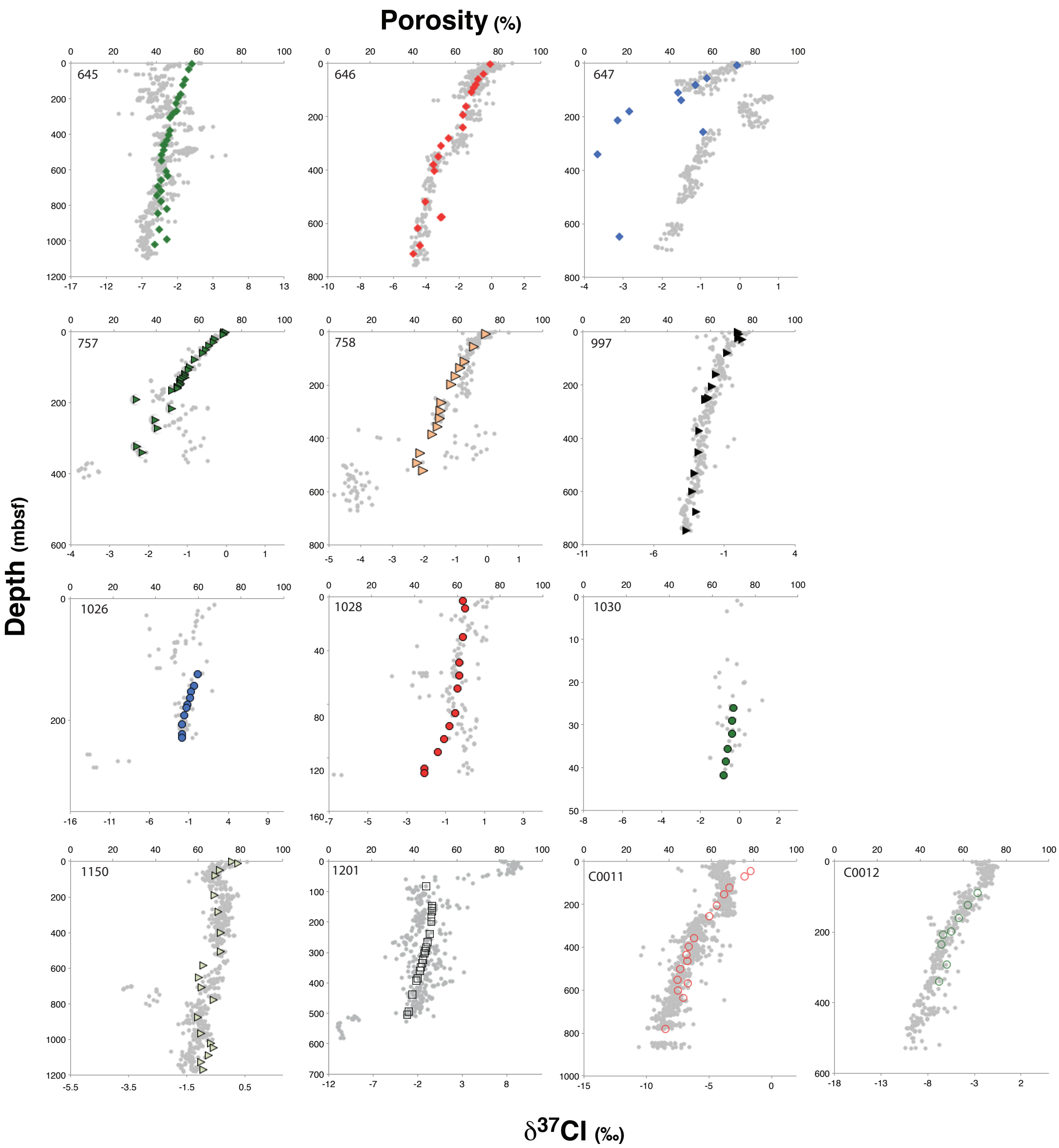


***Figure sup 1**: Porosity and $\delta^{37}$Cl depth profiles. Porosity data (small grey disks) are from ODP-IODP literature (Table 1). $\delta^{37}$Cl data (symbols as in previous figures) from data from Table of supplementary material. For 1201, C0011 and C0012, deviant trend data are not reported (see discussion in Agrinier et al., 2019).*

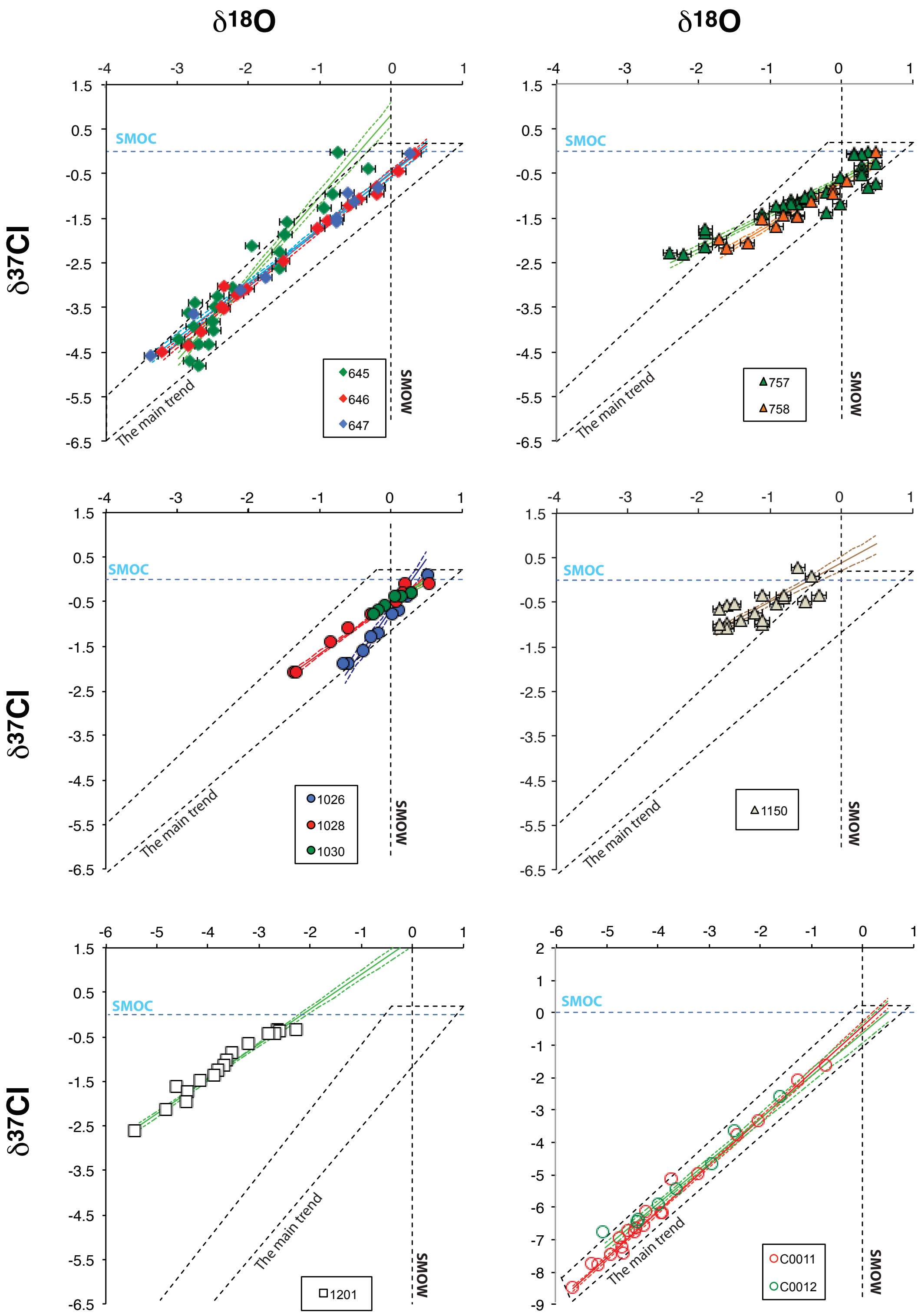


***Figure sup 2**: The $\delta^{37}Cl$– $\delta^{18}O$ relationship for each sedimentary pile. Least square Line (solid line) and 66 % confidence band for the line (dashed hyperbola) are reported. For Sedimentary piles 1201 and C0012, the sets of data were filtered to exclude outliers that result from external fluid influx (see Agrinier et al. (2019) for discussion). The $\delta^{37}Cl$–$\delta^{18}O$ relationship for Sedimentary pile 997 is not reported because it is poorly determined (r = 0.42).*

Table of the supplementary material

| Leg, Site, Hole, Core, Section, interval | Depth (mbsf) | Age (Ma) | Porosity | $Cl^-$ (mM) | $Na^+$ (mM) | $Ca^{2+}$ (mM) | $Mg^{2+}$ (mM) | $\delta^{18}O$ (‰) | $\delta^{37}Cl$ (‰) |
|---|---|---|---|---|---|---|---|---|---|
| 105-645B 1X2 140-150 | 2.9 | <0.73 | 0.58 | 549.09 | | 10.08 | 49.54 | -0.74 | -0.03 |
| 105-645B 5X2 140-150 | 35.1 | <0.73 | 0.44 | 526.39 | | 4.41 | 32.35 | -0.31 | -0.42 |
| 105-645B 11X2 140-150 | 93.8 | 0.73 | 0.45 | 545.62 | | 5.45 | 31.54 | -0.81 | -0.97 |
| 105-645B 14X3 140-150 | 124.3 | 0.98 | 0.44 | 535.98 | | 5.29 | 32.56 | -0.93 | -1.29 |
| 105-645B 19X3 140-150 | 172.5 | 0.65-1.6 | 0.38 | 553.78 | | 4.94 | 32.52 | -1.45 | -1.61 |
| 105-645B 21X5 140-150 | 194.8 | 0.65-1.6 | 0.40 | 493.75 | | 7.41 | 34.31 | -1.48 | -1.88 |
| 105-645B 24X5 140-150 | 223.6 | 0.65-1.6 | 0.49 | 559.9 | | 4.61 | 32.53 | -1.56 | -2.27 |
| 105-645B 30X6 140-150 | 283.1 | 1.6-3.4 | 0.49 | 482.86 | | 6.14 | 28.05 | -1.56 | -2.64 |
| 105-645D 1R3 140-150 | 269.8 | 1.6-3.4 | 0.45 | 538.46 | | 7.06 | 33.71 | -1.94 | -2.13 |
| 105-645D 8R2 140-150 | 304.7 | 1.6-3.4 | 0.40 | 582.94 | | 7.88 | 29.54 | n.a. | -3.04 |
| 105-645D 11R5 140-150 | 376.8 | 1.6-3.4 | 0.55 | 510.11 | | 7.48 | 26.9 | -2.22 | -3.08 |
| 105-645D 14R3 140-150 | 402.7 | 1.6-3.4 | 0.41 | 561.93 | | 7.51 | 28.19 | -2.43 | -3.26 |
| 105-645D 17R4 140-150 | 433.1 | 1.6-3.4 | 0.44 | 555.78 | | 7.59 | 27.57 | -2.47 | -3.49 |
| 105-645D 20R3 140-150 | 460.6 | 3.4 | 0.45 | 539.14 | | 8.03 | 26.66 | -2.48 | -4.04 |
| 105-645E 4R3 140-150 | 459.6 | 3.4 | 0.45 | 545.12 | | 7.73 | 26.91 | -2.49 | -3.84 |
| 105-645E 7R4 140-150 | 490 | 1.6-5.3 | 0.52 | 523.37 | | 8.42 | 25.83 | -2.77 | -3.94 |
| 105-645E 10R2 140-150 | 515.9 | 1.6-5.3 | 0.47 | 554.23 | | 9.13 | 24.03 | -2.98 | -4.25 |
| 105-645E 13R5 140-150 | 549.2 | 1.6-5.3 | 0.48 | 548.59 | | 9.69 | 20.52 | n.a. | -4.19 |
| 105-645E 19R4140-150 | 605.7 | 1.6-5.3 | 0.41 | 522.07 | | 10.51 | 24.75 | -2.83 | -3.64 |
| 105-645E 23R2 140-150 | 631.3 | 8.92 | 0.43 | 543.87 | | 10.73 | 22.28 | -2.74 | -3.42 |
| 105-645E 26R2 140-150 | 660 | 8.92-10.42 | 0.47 | 543.71 | | 11.97 | 21.27 | -2.7 | -4.34 |
| 105-645E 29R5 140-150 | 693.4 | 8.92-10.42 | 0.40 | 527.15 | | 12.95 | 18.97 | -2.81 | -4.73 |
| 105-645E 33R3 140-150 | 719.1 | 8.92-10.42 | 0.39 | 525.99 | | 14.93 | 20.72 | -2.83 | -4.36 |
| 105-645E 36R1 140-150 | 745.1 | <15 | 0.47 | 527.15 | | 13.86 | 18.29 | -2.69 | -4.84 |
| 105-645E 39R3 140-150 | 778.6 | <15 | 0.41 | 498.46 | | 14.15 | 18.24 | -2.55 | -4.34 |
| 105-645E 43R5 140-150 | 818.6 | <15 | 0.38 | 518.26 | | 18.06 | 15.65 | n.a. | -3.52 |
| 105-645E 46R3 140-150 | 844.5 | <15 | 0.37 | 506.9 | | 17.24 | 15.48 | n.a. | -4.8 |
| 105-645E 56R4 140-150 | 932.6 | <15 | 0.35 | 533.78 | | 15.8 | 16.04 | n.a. | -4.55 |
| 105-645E 62R5 140-150 | 991.6 | < 17 | 0.34 | 602.77 | | 18.14 | 16.34 | n.a. | -3.51 |
| 105-645E 65R5 140-150 | 1021 | 10.4 - 30 | 0.33 | 555.02 | | 16.38 | 13.6 | n.a. | -5.22 |
| 105-646A 1H3 140-15 | 4.4 | <0.2 | 0.74 | 565.82 | | 9.79 | 49.78 | 0.34 | -0.08 |
| 105-646A 7H5 140-150 | 61 | <1.75 | 0.71 | 550.59 | | 9.49 | 38.82 | -0.18 | -0.8 |
| 105-646A 10H4 140-150 | 90 | <1.75 | 0.69 | 546.64 | | 11.17 | 35.59 | -0.43 | -1.1 |
| 105-646B 5H2 140-150 | 39.8 | ≈ 0.475 | 0.72 | 557.64 | | 8.88 | 44.71 | 0.12 | -0.48 |
| 105-646B 9H5 140-150 | 79.8 | <1.75 | 0.70 | 573.15 | | 10.46 | 38.32 | -0.19 | -0.97 |
| 105-646B 12H3 140-150 | 107.3 | <1.75 | 0.65 | 551.72 | | 11.47 | 34.74 | -0.58 | -1.24 |
| 105-646B 18X2 140-150 | 162 | <2.4 | 0.66 | 568.08 | | 12.32 | 31.87 | -0.88 | -1.58 |
| 105-646B 21X4 140-150 | 194.1 | <3.5 | 0.63 | 564.97 | | 15.11 | 30.63 | -1.02 | -1.75 |
| 105-646B 26X4 140-150 | 242 | <3.5 | 0.61 | 571.74 | | 20.66 | 27.81 | -1.51 | -2.49 |
| 105-646B 30X4 140-150 | 280.9 | <3.5 | 0.62 | 567.23 | | 28.43 | 22.2 | | -2.61 |
| 105-646B 33X4 140-150 | 310 | <3.5 | 0.62 | 569.2 | | 34.51 | 17.99 | -2.01 | -3.1 |
| 105-646B 37X5 140-150 | 350.2 | <4.4 | 0.51 | 569.2 | | 46.29 | 11.03 | -2.16 | -3.25 |
| 105-646B 40X5 140-150 | 379.1 | <4.4 | 0.52 | 567.23 | | 49.6 | 10.21 | -2.34 | -3.55 |
| 105-646B 43X2 140-150 | 403.6 | <4.5 | 0.51 | 562.43 | | 54.46 | 9.88 | -2.37 | -3.51 |
| 105-646B 55X1 140-150 | 517.9 | 5.6 | 0.46 | 566.67 | | 60.45 | 9.53 | -2.65 | -4.07 |
| 105-646B 58X2 140-150 | 578.4 | <6.5 | 0.44 | 560.74 | | 55.77 | 13.59 | -2.09 | -3.16 |
| 105-646B 61X1 140-150 | 575.4 | 6.5 | 0.44 | 556.79 | | 56.6 | 13.54 | -2.33 | -3.04 |
| 105-646B 65X3 140-150 | 616.9 | <8.2 | 0.44 | 558.77 | | 61.88 | 6.08 | -3.2 | -4.52 |
| 105-646B 72X2 140-150 | 682.7 | <8.2 | 0.41 | 558.49 | | 58.24 | 7.78 | -2.84 | -4.39 |
| 105-646B 75X4 140-150 | 714.5 | <8.2 | 0.40 | 552.28 | | 58.72 | 7.06 | | -4.78 |
| 105-647A 1R5 140-150 | 7.4 | <0.247 | 0.73 | 539.59 | | 10.79 | 50.18 | 0.27 | -0.07 |
| 105-647A 6R5 140-150 | 56 | <1.9 | 0.62 | 555.67 | | 12.81 | 46.06 | -0.17 | -0.84 |
| 105-647A 9R2 140-150 | 82 | <1.9 | 0.54 | 563.28 | | 14.08 | 43.47 | -0.5 | -1.14 |
| 105-647A 12R3 140-150 | 111.1 | 2.4 | 0.55 | 555.1 | | 15.36 | 43.28 | -0.76 | -1.59 |
| 105-647A 15R2 140-150 | 138.3 | <30.3 | 0.83 | 545.51 | | 16.11 | 45.41 | -0.75 | -1.51 |
| 105-647A 19R5 140-150 | 181.2 | <34.6 | 0.75 | 553.69 | | 19.47 | 41.96 | -1.76 | -2.86 |
| 105-647A 23R2 140-150 | 215.2 | 34.6 | 0.80 | 555.67 | | 22.37 | 41.32 | -2.1 | -3.14 |
| 105-647A 27R5 140-150 | 257.8 | <36.8 | 0.60 | 560.18 | | 19.26 | 41.24 | -0.6 | -0.94 |
| 105-647A 36R3 140-150 | 341.6 | <38.5 | 0.58 | 530 | | 29.15 | 33.29 | -2.76 | -3.67 |
| 105-647A 39R2 140-150 | 369 | <38.5 | 0.55 | 540.43 | | 31.64 | 32.04 | -3.36 | -4.61 |

| Leg, Site, Hole, Core, Section, interval | Depth (mbsf) | Age (Ma) | Porosity | $Cl^-$ (mM) | $Na^+$ (mM) | $Ca^{2+}$ (mM) | $Mg^{2+}$ (mM) | $\delta^{18}O$ (‰) | $\delta^{37}Cl$ (‰) |
|---|---|---|---|---|---|---|---|---|---|
| 105-647A 67R2 140-150 | 649.4 | <53.6 | 0.40 | 524.64 | | 43.88 | 28.86 | | -3.14 |
| 121-757B 1H-2 140-150 | 2.7 | ≈ 1.5 | 0.74 | 542 | | 12.3 | 50.5 | 0.4 | -0.02 |
| 121-757B 3H-5 145-150 | 21.5 | ≈ 3 | 0.69 | 557 | | 23.8 | 46.8 | 0.5 | -0.28 |
| 121-757B 4H-4 148-150 | 29.6 | ≈ 4 | 0.65 | | | 28.8 | 44.5 | 0.3 | -0.33 |
| 121-757B 5H-4 148-150 | 39.2 | ≈ 4 | 0.64 | | | 33.2 | 42.6 | 0.3 | -0.44 |
| 121-757B 6H-5 145-150 | 50.3 | ≈ 5.5 | 0.62 | 575 | | 38.3 | 40.5 | 0.3 | -0.52 |
| 121-757B 7H-4 148-150 | 58.5 | ≈ 6.5 | 0.60 | | | 42.7 | 38.9 | 0 | -0.6 |
| 121-757B 8H-5 148-150 | 69.7 | ≈ 7.8 | 0.59 | | | 47.9 | 38 | 0.5 | -0.73 |
| 121-757B 9H-4 145-150 | 77.8 | ≈ 9.5 | 0.57 | 568 | | 51.9 | 34.8 | 0.4 | -0.82 |
| 121-757B 11H-5 148-150 | 98.7 | ≈ 20.5 | 0.56 | | | 61.9 | 31.5 | -0.2 | -0.93 |
| 121-757B 12H-5 145-150 | 108.5 | ≈ 28.5 | 0.55 | 577 | | 66.3 | 29.4 | -0.4 | -0.96 |
| 121-757B 13H-5 138-150 | 118 | ≈ 32 | 0.51 | | | 72 | 26.1 | -0.5 | -1.06 |
| 121-757B 14H-5 148-150 | 127.6 | ≈ 35.5 | 0.50 | | | 76.1 | 24.6 | -0.5 | -1.12 |
| 121-757B 15H-4 145-150 | 135.8 | ≈ 38.5 | 0.47 | 579 | | 79.5 | 23 | -0.6 | -1.16 |
| 121-757B 16H-4 148-150 | 145.5 | ≈ 39 | 0.43 | | | 84 | 22.1 | -0.6 | -1.17 |
| 121-757B 17H-5 148-150 | 156.6 | ≈ 42 | 0.47 | | | 91.3 | 18.2 | -0.8 | -1.26 |
| 121-757B 18H-5 145-150 | 166.3 | ≈ 44 | 0.42 | 583 | | 93.8 | 18.3 | -0.2 | -1.39 |
| 121-757B 21X-5 145-150 | 190.2 | ≈ 47.5 | 0.41 | 598 | | 103.1 | 15.7 | -2.2 | -2.31 |
| 121-757B 24X-4 140-150 | 217.7 | > 52 | 0.58 | 593 | | 109.6 | 9.1 | -1.1 | -1.4 |
| 121-757B 27X-5 140-150 | 248.2 | > 52 | 0.50 | 594 | | 124.9 | 0 | -1.9 | -1.83 |
| 121-757B 30X-2 140-150 | 272.7 | > 52 | 0.44 | 598 | | 131.6 | 0 | -1.9 | -1.76 |
| 121-757B 35X-CC 0-1 | 322 | > 52 | 0.56 | 604 | | 149.3 | 0 | -2.4 | -2.28 |
| 121-757B 37X-2 140-150 | 340 | > 52 | 0.35 | 598 | | 150.7 | 0 | -1.9 | -2.16 |
| 121-757C 1R-1 148-150 | 1.5 | 0.8 | 0.74 | | | 11.4 | 51.5 | 0.2 | -0.06 |
| 121-757C 1R-4 148-150 | 6 | 1.9 | 0.73 | 551 | | 12.8 | 51.3 | 0.3 | -0.08 |
| 121-757C 1R-6 148-150 | 9 | 2 | 0.72 | | | 13.2 | 51.5 | 0.2 | -0.07 |
| 121-757C 2R-1 148-150 | 123 | ≈ 33.5 | 0.50 | 581 | | 70 | 30 | -0.5 | -1.07 |
| 121-757C 2R-6 148-150 | 130.5 | ≈ 37 | 0.48 | | | 72 | 27.9 | -0.5 | -1.05 |
| 121-757C 3R-1 148-150 | 132.6 | ≈ 38 | 0.48 | 583 | | 75.7 | 26.7 | -0.7 | -1.11 |
| 121-757C 4R-1 148-150 | 142.3 | ≈ 39 | 0.46 | | | 79.4 | 25.3 | -0.7 | -1.19 |
| 121-757C 4R-6 148-150 | 149.8 | ≈ 40 | 0.45 | 571 | | 81.7 | 25.7 | 0 | -1.19 |
| 121-757C 5R-3 148-150 | 155 | ≈ 41 | 0.45 | n.a | | 85.1 | 23 | -0.8 | -1.23 |
| 121-757C 5R-6 148-150 | 159.5 | ≈ 43 | 0.44 | 589 | | 88 | 22.3 | -0.9 | -1.23 |
| 121-758A 1H3 145-150 | 4.5 | 0.47 | 0.76 | 547 | | 10.7 | 51.7 | 0.5 | -0.02 |
| 121-758A 6H6 145-150 | 53.35 | ≈ 3.6 | 0.67 | 563 | | 14.3 | 48.5 | | -0.4 |
| 121-758A 12X5 145-150 | 108.9 | ≈ 9 | 0.64 | 549 | | 17.5 | 46.1 | 0.1 | -0.68 |
| 121-758A 15X2 145-150 | 134.4 | ≈ 15 | 0.65 | 555 | | 20 | 45.3 | -0.1 | -0.83 |
| 121-758A 18X3 145-150 | 164.9 | ≈21 | 0.63 | 548 | | 21.8 | 44.2 | -0.1 | -0.97 |
| 121-758A 21X4 145-150 | 195.3 | ≈24 | 0.62 | 558 | | 23.4 | 43.5 | -0.4 | -1.12 |
| 121-758A 28X5 145-150 | 264.4 | ≈59 | 0.54 | 555 | | 28.1 | 40.8 | -0.6 | -1.43 |
| 121-758A 31X5 145-150 | 293.4 | ≈65 | 0.56 | 556 | | 30.7 | 39.7 | -0.8 | -1.44 |
| 121-758A 34X5 145-150 | 322.4 | >65 | 0.52 | 563 | | 33.5 | 37.9 | -0.6 | -1.46 |
| 121-758A 38X1 145-150 | 354.1 | >66 | 0.50 | n.a. | | 42.5 | 31.9 | -1.1 | -1.53 |
| 121-758A 41X4 140-150 | 383 | >67 | 0.74 | 566 | | 46 | 30.6 | -0.9 | -1.7 |
| 121-758A 50X4 140-150 | 452.1 | >68 | 0.60 | 548 | | 55 | 26 | -1.3 | -2.08 |
| 121-758A 54R1 140-150 | 490.7 | >68 | 0.57 | 574 | | 57.7 | 25.8 | -1.6 | -2.18 |
| 121-758A 57R1 140-150 | 519.4 | >68 | 0.40 | 585 | | 76.3 | 18.7 | -1.7 | -1.99 |
| 164-997A 1H-1 | 1.45 | < 0.3 | 0.72 | 558 | | 10.34 | 50.25 | 0.462 | -0.07 |
| 164-997A 2H-5 | 10.3 | 0.3 | 0.67 | 561 | | 6.19 | 42.56 | 0.27 | 0.08 |
| 164-997A 4H-1 | 23.3 | 0.7 | 0.65 | 558 | | 3.06 | 29.23 | 0.19 | 0.01 |
| 164-997A 4H-6 | 30.8 | 0.8 | 0.69 | 549 | | 2.65 | 25.91 | 0.15 | 0.26 |
| 164-997A 10H-6 | 79.65 | ≈ 1.7 | 0.68 | 536 | | 1.92 | 22.89 | 0.11 | -0.76 |
| 164-997A 20H-1 | 158.75 | ≈ 2.5 | 0.65 | 519 | | 2.65 | 21.42 | -0.24 | -1.59 |
| 164-997A 26X-1 | 204.75 | ≈ 2.9 | 0.63 | 512 | | 2.7 | 19.38 | | -1.88 |
| 164-997A 31X-4 | 246.7 | ≈ 3.2 | 0.60 | 469 | | 2.5 | 16.88 | -0.19 | -2.11 |
| 164-997A 32X-3 | 254.8 | ≈ 3.3 | 0.59 | 454 | | 1.35 | 13.68 | -0.22 | -2.2 |
| 164-997A 32X-4 | 255 | ≈ 3.3 | 0.60 | 500 | | 1.57 | 16.54 | -0.08 | -2.34 |
| 164-997A 32X-5 | 257.8 | ≈ 3.3 | 0.60 | 483 | | 1.95 | 16.29 | -0.49 | -2.36 |
| 164-997A 46X-5 | 372.9 | ≈ 4.4 | 0.56 | 492 | | 1.65 | 14.4 | -0.25 | -2.79 |
| 164-997B 8X-6 | 451.65 | ≈ 4.9 | 0.55 | 416 | | 2.03 | 10.41 | 0.22 | -2.85 |

| Leg, Site, Hole, Core, Section, interval | Depth (mbsf) | Age (Ma) | Porosity | $Cl^-$ (mM) | $Na^+$ (mM) | $Ca^{2+}$ (mM) | $Mg^{2+}$ (mM) | $\delta^{18}O$ (‰) | $\delta^{37}Cl$ (‰) |
|---|---|---|---|---|---|---|---|---|---|
| 164-997B 19X-2 | 532.35 | ≈ 5.4 | 0.54 | 512 | | 3.12 | 13.67 | -0.2 | -3.09 |
| 164-997B 28X-2 | 598.82 | ≈ 5.7 | 0.53 | 516 | | 4.82 | 15.05 | 0.28 | -3.27 |
| 164-997B 38X-2 | 676.55 | ≈ 6.0 | 0.48 | 517 | | 5.58 | 14.72 | 0.16 | -2.97 |
| 164-997B 47X-4 | 746.85 | > 6.0 | 0.48 | 512 | | 8.52 | 13.66 | -0.01 | -3.68 |
| 168-1026C 5R-1 135-150 | 124.5 | 0.4 | 0.62 | 575.13 | 497 | 18.24 | 22.59 | 0.53 | 0.1 |
| 168-1026C 7R-1 128-148 | 143.7 | 0.5 | 0.56 | 577.14 | 494 | 27.95 | 17.04 | 0.26 | -0.4 |
| 168-1026C 8R-1 68-78 | 152.7 | 0.6 | 0.66 | 574.73 | 492 | 31.08 | 13.68 | 0.12 | -0.7 |
| 168-1026C 9R-1 135-150 | 163 | 0.6 | 0.53 | 575.13 | 489 | 38.28 | 10.06 | 0.04 | -0.8 |
| 168-1026C 10R-2 135-150 | 174.1 | 0.7 | 0.50 | 575.13 | 488 | 46.1 | 6.44 | -0.16 | -1.2 |
| 168-1026C 10R-5 135-150 | 178.6 | 0.7 | 0.54 | 575.13 | 483 | 48.28 | 7.49 | -0.26 | -1.3 |
| 168-1026C 12R-1 130-150 | 191.9 | 0.8 | 0.51 | 570.14 | 472 | 53.79 | 6.77 | -0.37 | -1.6 |
| 168-1026C 13R-4 130-150 | 206 | 0.9 | 0.53 | 565.14 | 463 | 59.09 | 5.64 | -0.58 | -1.9 |
| 168-1026C 15R-3 59-79 | 223 | ≈ 1.4 | 0.53 | 568.63 | 463 | 60.33 | 5.76 | -0.59 | -1.9 |
| 168-1026C 15R-7 25-45 | 228.7 | > 1.4 | 0.57 | 564.13 | 453 | 62.82 | 6.02 | -0.65 | -1.9 |
| 168-1028A 1H-2 140-150 | 3 | ≈ 0.01 | 0.72 | 555.14 | 480 | 10.02 | 49.34 | 0.22 | -0.1 |
| 168-1028A 2H-3 150-160 | 8.3 | ≈ 0.02 | 0.72 | 560.64 | 482 | 9.1 | 45.97 | | 0 |
| 168-1028A 4H-5 140-150 | 30.2 | ≈ 0.1 | 0.68 | 571.14 | 490 | 7.2 | 40.36 | 0.56 | -0.1 |
| 168-1028A 6H-5 140-150 | 49.2 | 0.17 | 0.65 | 571.12 | 488 | 10.12 | 34.99 | 0.3 | -0.3 |
| 168-1028A 7H-5 140-150 | 58.7 | 0.21 | 0.59 | 572.87 | 491 | 11.55 | 32.87 | 0.18 | -0.3 |
| 168-1028A 8H-5 140-150 | 68.2 | 0.3 | 0.56 | 569.87 | 486 | 13.38 | 32.11 | 0.15 | -0.4 |
| 168-1028A 10H-5 135-150 | 87.1 | 0.41 | 0.57 | 572.11 | 488 | 22.24 | 27.69 | 0.09 | -0.5 |
| 168-1028A 11H-5 135-150 | 96.6 | 0.6 | 0.61 | 572.12 | 490 | 24.95 | 24.45 | -0.26 | -0.8 |
| 168-1028A 12H-5 135-150 | 106.1 | 0.84 | 0.58 | 571.61 | 485 | 30.79 | 22.51 | -0.59 | -1.1 |
| 168-1028A 13X-5 135-150 | 115.5 | 0.99 | 0.63 | 566.14 | 479 | 32.25 | 22.59 | -0.83 | -1.4 |
| 168-1028A 15X-3 135-150 | 128.2 | ≈ 1.2 | 0.65 | 568.08 | 480 | 34.44 | 20.78 | -1.36 | -2.1 |
| 168-1028A 15X-6 0-15 | 131.4 | ≈ 1.25 | 0.64 | 562.32 | 474 | 41.34 | 16.41 | -1.31 | -2.1 |
| 168-1030B 4H-2 140-150 | 26 | 0.26 | 0.69 | 574.34 | 489 | 57.03 | 6.7 | 0.3 | -0.3 |
| 168-1030B 4H-4 140-150 | 29 | 0.28 | 0.66 | 571.74 | 487 | 57.18 | 6.53 | 0.16 | -0.4 |
| 168-1030B 4H-6 140-150 | 32 | 0.36 | 0.70 | 571.4 | 488 | 57.57 | 5.86 | 0.07 | -0.4 |
| 168-1030B 5H-2 140-150 | 35.5 | 0.46 | 0.70 | 568.49 | 488 | 58.06 | 6.32 | -0.07 | -0.6 |
| 168-1030B 5H-4 140-150 | 38.5 | 0.57 | 0.65 | 567.63 | 486 | 59.54 | 5.81 | -0.16 | -0.7 |
| 168-1030B 6X-CC 0-20 | 41.7 | > 0.65 | 0.65 | 561.21 | 485 | 58.51 | 5.81 | -0.22 | -0.8 |
| 186-1150A 1H3 144–145 | 4.5 | ≈ 0.04 | 0.73 | 554 | 461.4 | 5.7 | 49.1 | -0.4 | 0.06 |
| 186-1150A 2H3 144–145 | 12.2 | ≈ 0.10 | 0.71 | 556 | 457.2 | 4 | 48.5 | -0.6 | 0.26 |
| 186-1150A 6H3 145–146 | 50.2 | 0.36 | 0.68 | 527 | 448.4 | 3.9 | 39.8 | -0.3 | -0.37 |
| 186-1150A 9H3 142–143 | 78.6 | 0.67 | 0.66 | 513 | 439.9 | 4.4 | 31.5 | -0.5 | -0.51 |
| 186-1150A 21X3 144–145 | 188.1 | 2.66 | 0.72 | 496 | 433.8 | 7.3 | 26.5 | -0.9 | -0.55 |
| 186-1150A 31X3 144–145 | 283.7 | 3.88 | 0.70 | 506 | 438.3 | 8.1 | 29.2 | -0.8 | -0.42 |
| 186-1150A 43X3 143–144 | 400.1 | 4.75 | 0.69 | 518 | 450.8 | 5.6 | 30.7 | -0.8 | -0.35 |
| 186-1150A 54X3 144–145 | 506.1 | 5.41 | 0.71 | 491 | 424.1 | 7.2 | 29.5 | -1.1 | -0.35 |
| 186-1150A 62X3 144–145 | 583.1 | 5.7 | 0.65 | 394 | 346.1 | 9.6 | 16.4 | -1.4 | -0.94 |
| 186-1150A 69X3 144–145 | 650.2 | 6 | 0.63 | 344 | 312.9 | 8.6 | 12.7 | -1.7 | -1.09 |
| 186-1150B 1R2 122–123 | 707.7 | 6.3 | 0.63 | 350 | 305 | 7.84 | 13.3 | -1.6 | -0.98 |
| 186-1150B 9R1 144–145 | 778.6 | 6.6 | 0.61 | 340 | 292 | 10.9 | 13.2 | -1.6 | -0.58 |
| 186-1150B 19R1 144–145 | 874.9 | 7 | 0.60 | 331 | 282 | 11.5 | 12.4 | -1.6 | -1.11 |
| 186-1150B 28R3 122–123 | 964.1 | 7.3 | 0.59 | 325 | 271 | 15 | 11.7 | -1.7 | -1.02 |
| 186-1150B 34R1 144–145 | 1018.9 | 7.9 | 0.58 | 318 | 263 | 16.5 | 10.9 | -1.7 | -0.67 |
| 186-1150B 37R1 144–145 | 1047.9 | 8.2 | 0.57 | 318 | 258 | 17.3 | 11.2 | -1.5 | -0.57 |
| 186-1150B 41R3 136–139 | 1089.6 | 8.8 | 0.57 | 307 | 250 | 17.2 | 10.2 | -1.2 | -0.75 |
| 186-1150B 45R2 139–140 | 1126.8 | ≈ 9.4 | 0.56 | 310 | 249 | 19.7 | 10 | -1.1 | -1.01 |
| 186-1150B 49R4 139-141 | 1168.2 | ≈ 9.5 | 0.56 | 324 | 258 | 21.4 | 10.3 | -1.1 | -0.94 |
| 195-1201D 1R-2 | 83.2 | ≥ 30 | 0.51 | 568.29 | 450 | 44.77 | 25.13 | | -1.08 |
| 195-1201D 7R-CC | 146.98 | ≈ 31 | 0.56 | 583.7 | 343 | 130 | 3.27 | -2.61 | -0.35 |
| 195-1201D 8R-4 | 153.21 | ≈ 31 | 0.53 | 594.64 | 342 | 136 | 2.05 | -2.56 | -0.38 |
| 195-1201D 9R-4 | 163.14 | ≈ 31 | 0.49 | 600.6 | 344 | 140 | 0.14 | -2.24 | -0.37 |
| 195-1201D 11R-5 | 183.41 | ≈ 31 | 0.41 | 608.6 | 327 | 156 | 0 | -2.66 | -0.44 |
| 195-1201D-13R-3 | 199.66 | ≈ 31 | 0.50 | 612.5 | 307 | 171 | 0 | -2.77 | -0.44 |
| 195-1201D 17R-3 | 238.04 | ≈ 31.6 | 0.53 | 625.46 | 255 | 197 | 0 | -3.17 | -0.67 |
| 195-1201D 20R-3 | 267.06 | ≈ 31.6 | 0.40 | 635.4 | 230 | 218 | 0 | -3.5 | -0.86 |
| 195-1201D 22R-1 | 283.52 | ≈ 31.6 | 0.47 | 633.4 | 224 | 217 | 0 | -3.6 | -1.05 |

| Leg, Site, Hole, Core, Section, interval | Depth (mbsf) | Age (Ma) | Porosity | $Cl^-$ (mM) | $Na^+$ (mM) | $Ca^{2+}$ (mM) | $Mg^{2+}$ (mM) | $\delta^{18}O$ (‰) | $\delta^{37}Cl$ (‰) |
|---|---|---|---|---|---|---|---|---|---|
| 195-1201D 23R-3 | 296.08 | ≈ 32.1 | 0.45 | 640.38 | 210 | 226 | 0 | -3.66 | -1.16 |
| 195-1201D 24R-1 | 302.88 | ≈ 32.1 | 0.49 | 636.4 | 217 | 223 | 0 | -3.77 | -1.27 |
| 195-1201D 26R-2 | 323.54 | ≈ 32.4 | 0.43 | 641.37 | 212 | 226 | 0 | -3.86 | -1.37 |
| 195-1201D 27R-3 | 334.22 | ≈ 32.5 | 0.47 | 642.37 | 215 | 227 | 0 | -4.13 | -1.48 |
| 195-1201D 28R-6 | 347.97 | ≈ 32.6 | 0.45 | 626.46 | 204 | 225 | 0 | -4.6 | -1.63 |
| 195-1201D 30R-1 | 360.6 | ≈ 32.7 | 0.39 | 640.38 | 191 | 237 | 0 | -4.36 | -1.75 |
| 195-1201D 32R-4 | 383.9 | > 32.7 | 0.44 | 646.3 | 197 | 239 | 0 | -4.4 | -1.99 |
| 195-1201D 33R-3 | 391.9 | > 32.7 | 0.45 | 643.9 | 188 | 243 | 0 | -4.8 | -2.14 |
| 195-1201D 38R-1 | 437.1 | > 32.7 | 0.43 | 648.3 | 159 | 260 | 0 | -5.4 | -2.62 |
| 195-1201D 44R-1 | 493.7 | > 32.7 | 0.39 | 651.3 | 162 | 257 | 0 | -4.2 | -3.05 |
| 195-1201D 45R-1 | 504.6 | > 32.7 | 0.37 | 660.3 | 152 | 275 | 0 | -3.6 | -3.20 |
| 322-C0011B 7R-3 | 395.1 | 8.1 | 0.51 | 561 | 497 | 25.3 | 4.8 | -4.26 | -6.63 |
| 322-C0011B 11R-4 | 434.6 | 8.6 | 0.54 | 561 | 497 | 26.6 | 4.6 | -4.44 | -6.81 |
| 322-C0011B 14R-4 | 463.1 | 8.9 | 0.50 | 550 | 486 | 27.6 | 3.9 | -4.57 | -6.76 |
| 322-C0011B 21R-2 | 501.6 | 9.7 | 0.45 | 545 | | | | -4.69 | -7.29 |
| 322-C0011B 26R-2 | 550.2 | 10.7 | 0.44 | 540 | | | | -4.92 | -7.53 |
| 322-C0011B 28R-2 | 569.5 | 11 | 0.44 | 547 | | | | -4.42 | -6.68 |
| 322-C0011B 32R-5 | 601.4 | 11.5 | 0.41 | 535 | 464 | 33 | 2.8 | -4.66 | -7.49 |
| 322-C0011B 36R-2 | 634.7 | 12 | 0.41 | 517 | 448 | 32.8 | 2.3 | -4.74 | -7.02 |
| 322-C0011B 43R-3 | 685.9 | 12.4 | 0.42 | 526 | 449 | 41.3 | | -3.92 | -6.23 |
| 322-C0011B 48R-3 | 722.5 | 12.8 | 0.36 | 509 | 423 | 44.5 | | -4.21 | -6.19 |
| 322-C0011B 53R-2 | 767.7 | 13.2 | 0.39 | 513 | 430 | 42.6 | 14.6 | -3.71 | -5.16 |
| 322-C0011B 55R-2 | 779.5 | 13.3 | 0.35 | 528 | 428 | 47 | 1.7 | -5.66 | -8.52 |
| 322-C0011B 57R-4 | 850.4 | 13.9 | 0.39 | 531 | 388 | 74.1 | | -5.17 | -7.84 |
| 322-C0011B 58R-3 | 858.3 | 14 | 0.36 | 542 | 398 | 74.1 | | -5.3 | -7.81 |
| 333-C0011D 3H-5 | 44.8 | 1.43 | 0.63 | 564 | 469 | 8.3 | 35.7 | -0.7 | -1.65 |
| 333-C0011D 6H-4 | 68.8 | 2.25 | 0.63 | 563 | 473 | 7.8 | 29.9 | -1.23 | -2.14 |
| 333-C0011D 13H-5 | 121.7 | 3.56 | 0.67 | 563 | 475 | 12.6 | 24.5 | -2 | -3.37 |
| 333-C0011D 17H-6 | 154.8 | 3.94 | 0.66 | 565 | 482 | 14.9 | 20.7 | -2.42 | -3.8 |
| 333-C0011D 26X-3 | 206.7 | 4.5 | 0.66 | 562 | 486 | 19.5 | 13.1 | | -4.36 |
| 333-C0011D 34X-4 | 254.4 | 5.38 | 0.59 | 555 | 480 | 23.5 | 10.6 | -3.2 | -5.01 |
| 333-C0011D 48X-3 | 356.5 | 7.2 | 0.53 | 554 | 486 | 27.6 | 4.9 | -3.9 | -6.22 |
| 322-C0012A 5R-2 | 89.4 | 5.1 | 0.63 | 561 | 480 | 24.4 | 35.7 | -1.58 | -2.61 |
| 322-C0012A 9R-4 | 124 | 7.4 | 0.62 | 562 | 481 | 31.8 | 22.4 | -2.47 | -3.67 |
| 322-C0012A 13R-2 | 159.6 | 7.9 | 0.56 | 555 | 468 | 38.5 | 14.6 | -2.93 | -4.69 |
| 322-C0012A 17R-3 | 198.8 | 8.6 | 0.52 | 565 | 466 | 46.5 | 7.6 | -3.62 | -5.5 |
| 322-C0012A 18R-2 | 207.9 | 8.7 | 0.52 | 556 | 450 | 49.4 | 6.1 | -4.38 | -6.41 |
| 322-C0012A 21R-2 | 235.4 | 10.9 | 0.51 | 560 | | 53.2 | 6.5 | -4.39 | -6.5 |
| 322-C0012A 27R-2 | 292 | 12.2 | 0.48 | 573 | 432 | 63.7 | 7.7 | -3.98 | -5.94 |
| 322-C0012A 32R-2 | 340.1 | 12.8 | 0.46 | 574 | 407 | 79.7 | 4.6 | -5.06 | -6.8 |
| 322-C0012A 37R-2 | 386.3 | 13.1 | 0.43 | 587 | 381 | 99.9 | 5.4 | -4.68 | -5.8 |
| 322-C0012A 43R-4 | 446 | 13.8 | 0.39 | 605 | 350 | 126 | 5.5 | -4.2 | -4.41 |
| 322-C0012A 45R-3 | 462.8 | 14 | 0.38 | 613 | 316 | 148 | 4.6 | -4.17 | -4.18 |
| 322-C0012A 48R-1 | 490 | 14.3 | 0.37 | 607 | 327 | 134.3 | 11.6 | -3.46 | -3.05 |
| 322-C0012A 50R-2 | 509.3 | >14.3 | 0.38 | 627 | 269 | 175.8 | 6.1 | -4.12 | -3.22 |
| 322-C0012A 52R-2 | 529.2 | >14.3 | 0.36 | 608 | 282 | 157.6 | 12.2 | -3.15 | -2.58 |

See Table 1 for references.